

DTIC FILE COPY

2

REPORT NO. NADC-90011-60



DTIC
ELECTE
JUL 06 1990
S D C D

**A LOW COST SHADOW MOIRE DEVICE FOR
THE NONDESTRUCTIVE EVALUATION OF
IMPACT DAMAGE IN COMPOSITE LAMINATES**

AD-A223 451

Arthur E. Scotese
Air Vehicle and Crew Systems Technology Department (Code 6041)
NAVAL AIR DEVELOPMENT CENTER
Warminster, PA 18974-5000

1 MARCH 1990

FINAL REPORT
Period Covering October 1987 to September 1988
Task No. R36200000
Work Unit No. ED801
Program Element No. 629361

Approved for Public Release; Distribution is Unlimited

Prepared for
Air Vehicle and Crew Systems Technology Department (Code 6041)
NAVAL AIR DEVELOPMENT CENTER
Warminster, PA 18974-5000

90 0 5 013

NOTICES

REPORT NUMBERING SYSTEM - The numbering of technical project reports issued by the Naval Air Development Center is arranged for specific identification purposes. Each number consists of the Center acronym, the calendar year in which the number was assigned, the sequence number of the report within the specific calendar year, and the official 2-digit correspondence code of the Command Officer or the Functional Department responsible for the report. For example: Report No. NADC 88020-60 indicates the twentieth Center report for the year 1988 and prepared by the Air Vehicle and Crew Systems Technology Department. The numerical codes are as follows:

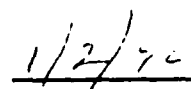
CODE	OFFICE OR DEPARTMENT
00	Commander, Naval Air Development Center
01	Technical Director, Naval Air Development Center
05	Computer Department
10	AntiSubmarine Warfare Systems Department
20	Tactical Air Systems Department
30	Warfare Systems Analysis Department
40	Communication Navigation Technology Department
50	Mission Avionics Technology Department
60	Air Vehicle & Crew Systems Technology Department
70	Systems & Software Technology Department
80	Engineering Support Group
90	Test & Evaluation Group

PRODUCT ENDORSEMENT - The discussion or instructions concerning commercial products herein do not constitute an endorsement by the Government nor do they convey or imply the license or right to use such products.

APPROVED BY:



DATE:



REPORT DOCUMENTATION PAGE

1a. REPORT SECURITY CLASSIFICATION UNCLASSIFIED		1b. RESTRICTIVE MARKINGS	
2a. SECURITY CLASSIFICATION AUTHORITY		3. DISTRIBUTION/AVAILABILITY OF REPORT Approved for public release; distribution is unlimited	
2b. DECLASSIFICATION/DOWNGRADING SCHEDULE		5. MONITORING ORGANIZATION REPORT NUMBER(S)	
4. PERFORMING ORGANIZATION REPORT NUMBER(S)		7a. NAME OF MONITORING ORGANIZATION N/A	
6a. NAME OF PERFORMING ORGANIZATION AIR VEHICLE AND CREW SYSTEMS TECHNOLOGY DEPARTMENT	6b. OFFICE SYMBOL (if applicable) 6041	7b. ADDRESS (City, State, and ZIP Code) N/A	
6c. ADDRESS (City, State, and ZIP Code) NAVAL AIR DEVELOPMENT CENTER WARMINSTER, PA 18974-5000		9. PROCUREMENT INSTRUMENT IDENTIFICATION NUMBER	
8a. NAME OF FUNDING/SPONSORING ORGANIZATION NAVAL AIR DEVELOPMENT CENTER	8b. OFFICE SYMBOL (if applicable) 6041	10. SOURCE OF FUNDING NUMBERS	
8c. ADDRESS (City, State, and ZIP Code) AIR VEHICLE & CREW SYSTEMS TECHNOLOGY DEPT WARMINSTER, PA 18974-5000		PROGRAM ELEMENT NO. 62936N	PROJECT NO. 0
		TASK NO. R36200000	WORK UNIT ACCESSION NO. ED801
11. TITLE (Include Security Classification) A LOW COST SHADOW MOIRE DEVICE FOR THE NONDESTRUCTIVE EVALUATION OF IMPACT DAMAGE IN COMPOSITE LAMINATES			
12. PERSONAL AUTHOR(S) ARTHUR E. SCOTSE <i>Shadow moire cut-off-plane Interferometric (SMOOP) Damage Detector</i>			
13a. TYPE OF REPORT FINAL	13b. TIME COVERED FROM 10/87 TO 9/88	14. DATE OF REPORT (Year, Month, Day) 1990 March 1	15. PAGE COUNT 30
16. SUPPLEMENTARY NOTATION - Interferometry			
17. COSATI CODES		18. SUBJECT TERMS (Continue on reverse if necessary and identify by block number)	
FIELD	GROUP	SUB-GROUP	
		Shadow Moire, impact damage, delaminations, composite structures, nondestructive testing, IED, optics,	
19. ABSTRACT (Continue on reverse if necessary and identify by block number)			
<p>Studies conducted under this Independent Exploratory Development (IED) project have concentrated on developing a field inspection instrument for the detection of low-velocity impact damage and delaminations in laminated composites and honeycomb sandwich structures. A low cost, hand-held battery-powered damage detector has been developed which can be operated under field conditions. This device can be used to detect minute surface perturbations resulting from foreign object impact that can cause disbond and/or delamination in aircraft structures. Since the operation of the device is simple and its detecting capability is not affected by temperature, humidity or vibration, it can be used under field operational conditions with minimum training. The entire detector system, including the power pack, weighs less than 3.5 lbs.</p> <p style="text-align: right;">Continued on back</p>			
20. DISTRIBUTION/AVAILABILITY OF ABSTRACT <input type="checkbox"/> UNCLASSIFIED/UNLIMITED <input checked="" type="checkbox"/> SAME AS RPT <input type="checkbox"/> DTIC USERS		21. ABSTRACT SECURITY CLASSIFICATION	
22a. NAME OF RESPONSIBLE INDIVIDUAL ARTHUR E. SCOTSE		22b. TELEPHONE (Include Area Code) (215) 441- 2396	22c. OFFICE SYMBOL 6041

19. Abstract (continued)

The device uses the basic principles of Shadow Moire Interferometry. When the structure is examined through a 4-inch x 5-inch viewing field, surface perturbations become visible in the form of Moire fringe patterns. The device is capable of detecting surface perturbations of less than 0.001 inch. The detector has proven to be practical, effective and reliable in detecting impact damage in composite laminate and honeycomb sandwich structures. Delaminations and disbonds have also been successfully detected. Damage sites can be scanned and identified quickly. If additional damage characterization becomes necessary, the flaw site can be further analyzed and quantified with other NDE techniques

Accession For	
NTIS CRA&I	<input checked="" type="checkbox"/>
DTIC TAB	<input type="checkbox"/>
Unannounced	<input type="checkbox"/>
Justification	
By	
Distribution /	
Availability Codes	
Dist	Avail and/or Special
A-1	



NADC-90011-60

TABLE OF CONTENTS

	PAGE
LIST OF FIGURES	iii
TABLE	v
FORWARD	vi
SUMMARY	vii
1.0 INTRODUCTION	1
2.0 MOIRE INTERFEROMETRY	1
2.1 In-Plane Displacements	1
2.2 Out-of-Plane Displacements	2
3.0 OBJECTIVE	2
3.1 Approach	2
4.0 INSTRUMENTATION AND EQUIPMENT	2
4.1 Shadow Moire Optical Bench	3
4.2 Shadow Moire Out-of-Plane Interferometric (SMOOPI) Damage Detector	3
5.0 TEST SPECIMENS	4
6.0 TEST PROCEDURE	4
6.1 General Methodology	4
6.1.1 Fatigue	4
6.1.2 Impact	4
6.2 Methods for Flaw Excitation	5
6.3 Sensitivity Enhancement via the Grid-Bias Linear Carrier-Fringe Method	5
7.0 MEASUREMENT AND DETECTION	6
8.0 DISCUSSION OF RESULTS	6
8.1 Moire Pattern Damage Correlation-Portable Optical Bench	6

NADC-90011-60

TABLE OF CONTENTS (Continued)

	PAGE
8.2 Moire Pattern Damage Correlation - SMOOPI Damage Detector Development	7
8.2.1 Description of Prototype SMOOPI Damage Detector	7
8.2.2 Experimental Results and Performance	8
8.2.3 Damage Quantification	9
9.0 SENSITIVITY ENHANCEMENT TECHNIQUES	9
9.1 Grid-Bias Linear Carrier-Fringe Method - Optical Bench	9
9.2 Carrier Fringes - with SMOOPI Damage Detector	9
9.3 Evaluation of Flaw Excitation Methods	10
9.3.1 Detecting Delaminations by Local Heating	10
9.4 Digital Image Processing	11
9.5 Additional Applications	12
10.0 CONCLUSIONS/RECOMMENDATIONS	12
10.1 Transition	13
REFERENCES	14

NADC-90011-60

LIST OF FIGURES

FIGURE		PAGE
1	Moire Fringe Analysis: Superposition of Master and Specimen Grids	16
2	Shadow Moire: Schematic Diagram of Setup	16
3	Portable Shadow Moire Optical Bench	17
4	Displacement Per Fringe For SMOOPI Damage Detector	19
5	Moire Fringes (3) About Lower Hole, After Fatigue Cycling, Inspected with 500 lpi Grid: 25 Ply GR/EP Specimen: Out-Of-Plane Displacement 0.003 Inch	20
6	Moire Fringes (2), After Impact Testing 40 Ply GR/EP Specimen, 0.02 Inch Out-Of-Plane Displacement	21
7	Moire Fringes (4), After Impact Testing: 40 Ply GR/EP Specimen, 0.04 Inch Displacement	22
8	SMOOPI Portable Damage Detector Being Used to Inspect AV-8B Stabilator for Impact Damage	23
9	SMOOPI Damage Detector Showing Non-Visible Impact Damage: 0.04 Inch Displacement	24
10	SMOOPI Damage Detector Showing Non-Visible Impact Damage: 0.001 Inch Displacement	25
11	Photomicrographs (100X) of 40 Ply GR/EP Specimen After Impact Damage, Note Delaminations	26
12	SMOOPI Damage Detector Showing Out-Of-Plane Displacement of Top Surface Resulting from Back-Surface Shattering	27
13	Shadow Moire Out-Of-Plane Interferometric (SMOOPI) Damage Detector with Battery-Pack, Charger & AC Adapter	28
14	SMOOPI Damage Detector Kit	29
15	Spherically Shaped Impact Damage, Three Fringes, .01 Inch Per Fringe Displacement, 50 lpi Grid, 63.5° Incidence Angle	30

NADC-90011-60

LIST OF FIGURES (Continued)

FIGURE		PAGE
16	Three Fringes - Elliptically Shaped Surface Contours 150 lpi Grid, 45° Incidence Angle, .0067 Inch-Per-Fringe Displacement, Viewed After Impact	31
17	Damage Displacement Profiles for Figures 15 & 16	32
18	Three Fringes - 250 lpi Grid, 63.5° Incidence Angle, .002 Inch-Per-Fringe Displacement, Viewed After Impact	33
19	Ultrasonic C-Scan of Specimen in Figure 18	34
20	Gird-Bias Linear Carrier Fringes: Moire Fringes With Out-Of-Plane Grid Rotation to Increase Sensitivity, After Impact; 50 Ply GR/EP Specimen	35
21	Carrier Fringes - 1/1/2 Fringe Order (out-of-line movement at center) 150 lpi Grid, 45° Angle of Incidence	36
22	Grid-bias Linear Carrier Fringes: 40 Ply GR/EP Specimen Viewed After Impact. 250 LPI Grid, 63.5° Angle of Incidence. Visual Sensitivity for 1/4 Fringe Interpolation Equals .0005	37
23	Low and High Order Displacement Area - 1+1/2 and 4 Fringes, 150 lpi Grid, 63.5° Incidence Angle, .0033 Inch-Per-Fringe Displacement	38
24	Moire Fringes Generated After 400° F Heat Excitation of Suspected Flaw Area	39
25	Computerization System	40
26	Digital Image Processing System	41
27	Color Program for 10X Resolution Enhancement for Digital Image Processing	42
28	Digital Image Processing - Line Program for Determination of Out-Of-Plane Deformation Profile	43
29	Displacement Profile (inches)	44
30	Photographic System for SMOOPI Damage Detector	45
31	Cold-Worked Holes in a Metal Plate - A Fringe is Visible at Each of the Cold-Worked Holes	46
32	Minute Blisters in an Anti-Corrosion Paint - Visible with 150 lpi Moire Grid	47

NADC-90011-60

TABLE

TABLE		PAGE
1	Displacement Per Fringe for SMOOPI Damage Detector	18

FOREWORD

This report presents the results of a two-year Independent Exploratory Development (IED) effort aimed at the development of a non-destructive methodology, suitable for use under field conditions, for the detection of impact damage and the surface manifestation of sub-surface fatigue damage in laminated structural composites and honeycomb sandwich structures using Shadow Moire interferometry. Efforts were directed toward the development of a field inspection instrument capable of detecting surface anomalies of 0.001 inch or less, unaffected by temperature and humidity variations or vibrational disturbances. The Author would like to thank his colleagues Dr. S. L. Huang, Joseph J. Minecci, Armando Gaetano, Glenn Werczynski and Gwynn McConnell of the NAVAIRDEVCON for their technical assistance and thoughtful comments during the program.

SUMMARY

Studies conducted under this Independent Exploratory Development (IED) project have concentrated on developing a field inspection instrument for the detection of low-velocity impact damage and delaminations in laminated composites and honeycomb sandwich structures. A low cost, hand-held battery-powered damage detector has been developed which can be operated under field conditions. This device can be used to detect minute surface perturbations resulting from foreign object impact that can cause disbond and/or delamination in aircraft structures. Since the operation of the device is simple and its detecting capability is not affected by temperature, humidity or vibration, it can be used under field operational conditions with minimum training. The entire detector system, including the power pack, weighs less than 3.5 lbs.

The device uses the basic principles of Shadow Moire Interferometry. When the structure is examined through a 4-inch x 5-inch viewing field, surface perturbations become visible in the form of Moire fringe patterns. The device is capable of detecting surface perturbations of less than 0.001 inch. The detector has proven to be practical, effective and reliable in detecting impact damage in composite laminate and honeycomb sandwich structures. Delaminations and disbonds have also been successfully detected. Damage sites can be scanned and identified quickly. If additional damage characterization becomes necessary, the flaw site can be further analyzed and quantified with other NDE techniques

1.0 INTRODUCTION

The application of cyclic loads to a structure can produce damage which propagates progressively and finally leads to catastrophic failure. The failure modes of composite structures differ considerably from those of metal structures. With metals, fatigue cracks are visible and initiate in the plane normal to the outer surface. With composites, however, damage often initiates and propagates internally, parallel to the laminate plane (References 1,2,3,4,5). Propagation of delamination is a major problem and has been responsible for the ultimate failure of composite laminates. Certain types of flaws in composite structures, such as low velocity impact damage (Reference 6), are not readily observable by visual examination. Other examples include blind-side and subsurface interlaminar cracks.

The increased use of laminated composites and honeycomb sandwich structures on naval aircraft has necessitated the development of inspection techniques to detect the presence and criticality of cracks, flaws, disbonds, delaminations and other defects. These inspections help to ensure that composite structures provide the same level of structural reliability as comparable metal structures. A variety of non-destructive methods are currently employed to detect internal damage in laminates (References 7,8). Ultrasonics and X-ray are commonly used in industrial applications. Thermographic, laser holography, acoustic emission, and simple hammer tapping have demonstrated varying degrees of applicability in experimental and field quality control programs. These methods can be tedious, time consuming and unreliable in field assignments where temperature, humidity and vibration can severely affect the results.

The availability of a more effective means for field detection of impact and resultant delamination is one of the major requirements for the extensive use of structural composites in aircraft today.

2.0 MOIRE INTERFEROMETRY

2.1 In-Plane Displacements

Moire Interferometry (References 9,10,11) has been well developed for in-plane displacements. The basic technique deals with the interference fringes created by the superposition of two grids or systems of finely ruled lines, one on the specimen and the other a master or reference grid. The specimen grid is either printed on, bonded to, or etched on the surface. The superposition of the reference and the specimen grid (Figure 1) is done either by direct contact or by imaging one onto the other via a lens. When subjected to mechanical forces, the test specimen is deformed and the specimen grid along with it. Because of the surface strains and resultant change in pitch (line to line distance) of the specimen grid rulings, Moire fringes are produced as a result of transmission and obstruction of light passing through the deformed and undeformed grids. The Moire fringes which represent the loci of points of constant displacement in a direction normal to the grid lines appear as black bands, because light transmitted by one set of opaque lines is obstructed in some regions by the other set. When the lines of the master

NADC-90011-60

grid coincide in some areas with the spaces of the specimen grid there is obstruction of light and Moire fringes are produced. The grid density in lines per inch (lpi) is usually small, e.g., 150 lpi to 1000 lpi, and individual lines are not seen.

2.2 Out-of-Plane Displacements

Shadow Moire is also based on interferometry and the superposition of two grids, but in this case, the specimen grid is the shadow of the master grid on the specimen surface (References 12,13). The Shadow Moire technique deals with the measurement of out-of-plane displacements or the out-of-plane shape of structures, rather than in-plane deformation. In a typical Shadow Moire set-up (Figure 2), a Master grid, is placed close to the examined surface and illuminated at some angle θ from 30° to 75° , and a shadow of the grid is projected on the surface. The shadows, i.e., the specimen grid, are distorted by the out-of-plane elevation or depth of the surface and when viewed through the master grid produce fringes which are clearly visible. A set of visible fringes is a map of level lines revealing the topography of the observed surface. When the specimen is deformed, the pitch of the shadow grid changes. When the lines on the master grid project onto lines on the specimen, reflection of the light path occurs. In some regions, however, the lines of the master obstruct the light reflected by the specimen and black Moire fringes appear.

3.0 OBJECTIVE

The objective of this IED program was to develop a non-destructive methodology, suitable for use under field conditions, for the detection of impact damage and the surface manifestation of sub-surface fatigue damage in laminated structural composites and honeycomb sandwich structures using Shadow Moire Interferometry.

3.1 Approach

The use of Shadow Moire Interferometry for detection of minute out-of-plane displacements resulting from impact and fatigue damage was investigated in this program. Efforts were directed toward the development of a field inspection instrument able to detect surface anomalies of 0.0001 inch or less, unaffected by temperature and humidity variations or vibrational disturbances.

4.0 INSTRUMENTATION AND EQUIPMENT

The development of the instrumentation was directed toward the identification of key design parameters, e.g., the focal distance of lenses, grid densities, illumination requirements, magnification factors, Moire screen dimensions, and photographic methods, and also the evaluation of several candidate sensitivity enhancement techniques including digital image processing.

NADC-90011-60

4.1 Shadow Moire Optical Bench

The initial, or baseline, system was intended for use in the laboratory, with emphasis on the capability to vary and determine the key design parameters of the system. It incorporated the following equipment and features:

- a. A portable optical bench (Figure 3) mounted on a heavy-duty, caster-equipped base with foot lock for easy maneuverability about the Fatigue Lab and Test Floor.
- b. Angle of incidence and height adjustments for proper shadow projection.
- c. A collimating point light source (500-watt) with adjustable slit width.
- d. Shadow Moire Screens 8 inches X 10 inches, 4 inches X 5 inches, 4 inches X 4 inches, and 1 inch X 2 inches, with densities ranging from 50 to 3000 lines per inch (lpi).
- e. A micrometer-controlled screen holder for attaching the screen to the bench support stand to avoid interactions. The three-point micrometer support was designed to control zero pattern, mismatch pattern and initial setting.

4.2 Shadow Moire Out-of-Plane Interferometric (SMOOPI) Damage Detector

Later in the program, a portable field inspection apparatus was developed, incorporating the optimum design parameters determined from the Shadow Moire Optical Bench experiments. The so-called SMOOPI device consists of the apparatus listed below:

- a. 4-inch X 5-inch 50, 150, 250 and 500 lpi Moire screens.
- b. 35-watt light source with adjustable-slit-width aperture.
- c. Angular-adjustable light source support.
- d. Three-point surface contact system.
- e. Pistol grip.

See the Discussion of Results section for details of the description and use of this device.

NADC-90011-60

5.0 TEST SPECIMENS

Fatigue and impact specimens were fabricated from stock material for use in this program. The fatigue specimens were 25-ply graphite/epoxy (Gr/Ep) (AS4-3501) laminates (18 inches X 1.5 inches X .125 inches) with a central transverse .25-inch diameter hole. They were prepared for Moire evaluation by fatigue testing in a 20-kip MTS Systems Corporation closed-loop servo-controlled electro-hydraulic test machine.

Impact specimens consisted of 4-inch X 4-inch 40-ply and 6-inch X 6-inch 25-ply Gr/Ep (AS4-3501) laminates. They were impact tested using a Dynatup Model 8200 drop tower with Dynatup Model 371 instrumented impact system. This tower can impose impact energies in the range from 1 to 320 foot-pounds, so a broad spectrum of composite damage could be evaluated. Each Gr/Ep plate was clamped in the drop tower along its edges and impacted with a 1/2-inch-radius hemispherical steel indenter. All specimens were inspected by ultrasonic C-SCAN before and after each test. Three types of impact specimens were produced:

- a. Specimens with some visible damage.
- b. Specimens with no visible damage but C-SCAN-detectable damage.
- c. Specimens with no visible damage and no C-SCAN damage.

6.0 TEST PROCEDURE

6.1 General Methodology

The Shadow Moire Optical Bench and SMOOPI Field Inspection Apparatus were evaluated by inspecting both fatigue and impact specimens for damage.

6.1.1 Fatigue

In the case of the fatigue specimens, a 20-kip MTS machine was used for constant-amplitude reversed cyclic loading of Gr/Ep coupons with a central through-the-thickness hole. The specimens were fatigue tested and inspected every 1000 cycles in search of a Moire metamorphosis or deformed fringe shape about the hole. It was observed that reversed cyclic loading tended to exaggerate the thickness change above damaged areas by inducing some localized buckling.

6.1.2 Impact

Impact specimens with varying degrees of damage, as determined by ultrasonic C-SCAN, were inspected with the Shadow Moire optical instrumentation. The Moire grid was adjusted with micrometer supports to be nearly parallel to the specimen surface. In order to verify that the observed fringe patterns did in fact correspond to internal damage

NADC-90011-60

in the laminate, cross-sections were cut from the laminate, polished, microscopically examined and photographed at a 100X magnification.

6.2 Methods for Flaw Excitation

In an attempt to extend the damage detection capability of the Moire instrumentation by inducing a small out-of-plane displacement at suspected flawed localities, the following flaw excitation methods were evaluated:

- a. Mechanical probing forces;
- b. Thermal shock or steady-state heating, either broad-area or local to the suspected flaw;
- c. Vibratory excitation of a possible flawed locality.

Mechanical forces were applied to the suspected flaw areas manually, using a blunt probe. Heat was applied to broad areas of the specimens via high-intensity lamps, and locally by means of a hot-air gun. For vibratory excitation, a speaker system was used for wide-area inputs.

In order to better evaluate the proposed excitation methods, a Gr/Ep specimen was prepared with 1-inch X 1-inch TEDLAR film pieces embedded between various layers to simulate delaminations.

6.3 Sensitivity Enhancement via the Grid-Bias Linear Carrier-Fringe Method

In performing out-of-plane Shadow Moire studies, it was noted that it is possible to increase the sensitivity of the technique and eliminate the ambiguity inherent in a low signal by creating an "error signal" or linear carrier fringe pattern. This is done by biasing the reference grid, i.e., tilting the grid forward a few degrees relative to the specimen plane. Any deformation in the specimen will produce a perturbation of the induced carrier fringes, resulting in an out-of-line movement or change in spacing of parallel fringes. When the undeformed fringe order is subtracted from the perturbed carrier fringe order, the true fringe order and corresponding deformation is obtained.

The Grid-Bias Linear Carrier-Fringe Method being developed herein is similar to the Grid Mismatch technique widely used with the in-plane Moire method. With the latter technique, instead of using a Master grid with a line-pitch identical to that of the specimen grid, a Master grid is used whose line frequency exceeds that of the specimen by a small line-density factor. Then, when the two grids are aligned, a pattern of straight parallel uniformly-spaced fringes similar to carrier fringes is formed, giving an apparent initial "strain" or error-signal. The displacements introduced by the specimen deformation are then added to this apparent strain.

7.0 MEASUREMENT AND DETECTION

The sensitivity of the system and "motion" of the shadows is based on the selected illumination angle, grid density and the elevation or depth of the observed point. The classic equation of the Shadow Moire technique is:

$$Z = 1/(P \times \tan \theta) \quad \text{Equation 1}$$

where Z is the level difference from one fringe to the next fringe, P is the grid density in lines per inch (lpi) and θ is the angle of incidence between the light source and the normal to the specimen surface. Using a 45° illumination angle, $\tan \theta = 1$ and $Z = 1/P$.

The light source is usually set at a 45° angle of incidence for most applications, but other angular settings are possible as indicated on the mounting bracket. When an increase in sensitivity is required, a 63.5° angle of incidence can be selected that will double the output of the 45° selection, or a grid with greater line density can be selected. Table I contains the displacement-per-fringe values for all available grid line densities and angles of incidence, and this information is presented graphically in Figure 4.

8.0 DISCUSSION OF RESULTS

8.1 Moire Pattern Damage Correlation - Portable Optical Bench

Shadow Moire Interferometry was used to observe damage initiation and propagation during fatigue cycling and impact testing. Interpretation of the Moire patterns in the attached figures is simplified if one recalls that each fringe line shows an increment of minute out-of-plane displacement and each display represents a contour map of surface topography. Discontinuities in the contour lines occur at locations where back-surface cracks or through-the-thickness ply failures occur.

Figure 5 shows the Moire fringe patterns and fatigue damage around a hole in a 25-ply GR/EP specimen when viewed with a 500-lpi grid at a 63.5° illumination angle. Three distinct fringes are visible, corresponding to an out-of-plane deformation of .003 inch, i.e., $Z=.001$ inch, from Equation 1. Figures 6 and 7 show non-visible impact damage as viewed with a 50 lpi Moire grid, (63.5° illumination angle) corresponding to deformations of .01 inch per fringe.

Although grid densities of up to 3000 lpi were evaluated, 1000 lpi was the maximum grid density found to be practical. Beyond this grid density, severe diffraction effects were encountered and fringe orders were obscured. The best results were obtained with grid densities of 150 to 500 lpi.

8.2 Moire Pattern Damage Correlation - SMOOPI Damage Detector Development

The data obtained from the portable optical bench were used to design and fabricate a breadboard model of the SMOOPI Damage Detector. The instrument is shown in Figure 8 being used to examine the AV-8B graphite/epoxy stabilator. It consists of a metal frame on a pistol grip, with attachments for a Moire grid, providing a .030-inch clearance between the grid and the surface to be examined. A battery-operated collimated light source with an adjustable slit width for Shadow Moire projection was attached to the frame by a swiveled jackknife linkage for angle and length changes. A three-point contact system was also incorporated into the frame, to accommodate inspection of curved surfaces, and to create a grid-bias-linear-carrier for sensitivity enhancement.

The SMOOPI Damage Detector showed itself to be capable of detecting out-of-plane surface anomalies of .0001 inch. Figures 9 and 10 show the Moire fringe patterns associated with non-visible impact damage of .002-inch and .001-inch displacement, using 250-lpi and 500-lpi grids respectively. Photomicrographs (100X magnification), Figure 11, of the suspected damaged area show distinct delaminations emanating from the point of impact. Figure 12 shows a typical pattern associated with blind-side impact damage or back-surface shattering, where the damage is not visible from the front surface. The damage in this area produced an out-of-plane movement on the top surface of less than .001-inch. The fringe pattern shows the deformation created by the split on the back surface.

8.2.1 Description of Prototype SMOOPI Damage Detector

The re-designed SMOOPI Damage Detector shown in Figure 13, consists of an anodized aluminum frame on an extended pistol grip with attachments for easy installation of a 4-inch x 5-inch Moire grid, providing a .030-inch clearance between the grid and the surface to be examined. A 35 watt quartz light source with a .050-inch slit provides a collimating line source, simulating a remote point, and is attached to the frame with a 6-inch support for simple adjustments of illuminator angle and vertical position. The light source can be powered from a portable, shoulder-strap-mounted, rechargeable battery-pack or from an AC adapter. The light source with battery-pack can last for one hour of continuous operation before recharging. The entire detector system including the battery-pack weighs less than 3.5 lbs.

Grids with line densities up to 1000 lpi were successfully used with the SMOOPI device. Severe diffraction effects, with the fringe orders being obscured, occurred with grid line densities greater than 1000 lpi. The best results were obtained with grid line densities of 50, 150, and 250 lpi. The 150 lpi grid is for general purpose applications and is used in most cases. A low and high density grid can also be used when required. For cases with too high a signal or poor contrast, the 50 lpi grid should be used. For cases with low displacement fields, the 250 lpi grid is appropriate and provides the best signal. A three-point contact system is also incorporated into the frame to accommodate inspection of curved surfaces and to produce an out-of-plane rotation of the master grid that creates a grid-bias or carrier fringe pattern (series

NADC-90011-60

of parallel lines) for sensitivity enhancement. The surface to be examined should be diffusely reflecting light. For surfaces with poor contrast, a white spray powder (Fluorofinder FD-33 Developer or equivalent) is used to increase contrast during inspection. The powder is then easily cleaned from the surface after inspection. A kit with additional grids, spray powder, cleaner, gauze pads, battery pack, charger and AC adapter (Figure 14) was assembled for use in the field.

When compared to other Non-Destructive techniques, the major advantages of the SMOOPI device are:

Low cost

Portable and light weight

Needs no specimen grid.

Scans large areas at a time.

8.2.2 Experimental Results and Performance

When using the SMOOPI Damage Detector, the frame is placed in contact with and parallel to the surface to be examined. On a flat surface with no damage, a zero pattern without any fringes is observed. For this condition, the pitch of the master grid and shadow remain the same. If the surface has a slight warpage or curvature, a series of equidistant parallel fringes are observed. Each fringe indicates a change in pitch between the master grid and specimen grid (shadow). In areas displaying one or more closed fringes (where each fringe or pitch change is a line of constant displacement), the general shape of the damage and a contour map of level lines revealing the surface topography will become visible. For example, spherically shaped damage areas will reveal a fringe pattern of concentric circles. This is shown in Figure 15, where using a 50 lpi grid and a 63.5° incidence angle, three concentric fringes are visible having a .01 inch-per-fringe displacement. In Figure 16, two fringes with slight perturbations and three closed fringes are visible representing a displacement of .0067 inch-per-fringe. In this case, the specimen was viewed with a 150 lpi grid at a 45° angle of incidence. The damage area profile for both impact fringe patterns is shown in Figure 17. This was done by drawing vertical lines thru each fringe that intersected the horizontal line drawn thru the center of the damaged area. The increase in pitch from one fringe to the next is plotted for each line giving a displacement profile of the cross-section.

For a 50 lpi density at a 45° illumination angle, one fringe represents a locus of points of equal out-of-plane displacement of .02 inch, as determined from Equation 1 or shown in Figure 4 or Table I. Using the general purpose grid of 150 lpi density, one fringe is equal to .0067 inch displacement at a 45° illumination angle. The sensitivity may be increased to .0033 inch per fringe at a 63.5° angle of incidence. For a 250 lpi grid at a 63.5° illumination angle, the sensitivity can be increased to .0020 inch of displacement per fringe (see Figure 4 or Table I). On a curved surface, fringes will also reveal the surface topography.

NADC-90011-60

For example, a curved surface will show a set of lines parallel to its axis. In this case, surface anomalies will be more difficult to observe, so it is very important to completely understand the shape of the zero or baseline contours.

8.2.3 Damage Quantification

Surface damage detection (References 14,15,16,17) with SMOOPI provides a means for fast inspection of large areas. For example, a 36 inch x 36 inch area can be easily inspected in a few minutes. After surface perturbations have been identified, the area can be A-Scanned or C-Scanned, if necessary, to further quantify flaw extent. This approach is demonstrated in Figures 18 and 19. A 25 ply graphite/epoxy specimen was inspected with the SMOOPI Damage Detector and three damage points were identified. One of the points, which is typical of the three, is shown in Figure 18, where three fringes are visible indicating an out-of-plane displacement profile of .002 inch per fringe. A 250 lpi grid and a 63.5° illumination angle were used. The specimen was then C-Scanned (Figure 19), revealing subsurface damage and the size of the delamination at each of the three points.

9.0 SENSITIVITY ENHANCEMENT TECHNIQUES

9.1 Grid-Bias Linear Carrier-Fringe Method - Optical Bench

Sensitivity enhancement via the Grid-Bias Linear Carrier-Fringe Method was also evaluated on the Portable Optical Bench, with considerable success. Figure 20 shows the Moire fringe patterns associated with an out-of-plane rotation of a 50 lpi grid at a 63.5° illumination angle. In this case, the Grid-Bias Linear Carrier-Fringe technique was used to artificially generate fringes in a small displacement field. The out-of-line movement from parallel straight lines represents damage, giving a qualitative visual determination of the deformation profile.

9.2 Carrier Fringes - with SMOOPI Damage Detector

A simple approach to increase sensitivity and eliminate the ambiguity associated with a low order displacement field, is to use the three-point contact system attached to the frame to form a plane which is tilted slightly from the master grid plane. For this type application, the frame is placed initially at a small angle (a few degrees out-of-plane) to the surface by adjustment of the contact screws on the frame, and on a flat surface, a pattern of equidistant parallel fringes (carrier fringes) is observed. A carrier fringe pattern of approximately two fringes per inch is adequate for most applications. If any surface perturbations are present, the parallelism of the carrier fringes will be disturbed in areas exhibiting less than one fringe, and the fringes will deform out-of-line as shown in Figure 21. A fringe order of $1/2$ magnitude can be easily interpolated by eye. In this case, using a 150 lpi grid and a 45° incidence angle, the elevation lines appear in .0067 inch-per-fringe increments. Interpolating 1 and $1/2$ fringes, the depth sensitivity in a direction perpendicular to the grid is .01 inch. Using a high density grid of 250 lpi and a 63.5° incidence angle, Figure 22, the depth increase for

NADC-90011-60

one fringe is .0020 inch and the visual sensitivity with a 1/4 fringe interpolation is .0005 inch. The contrast between a low damaged area and a high damaged area is shown in Figure 23, where a 150 lpi density grid and a 63.5° angle of incidence were used. For this case, one and one-half fringes and four fringes are displayed with a .0033 inch displacement per fringe.

9.3 Evaluation of Flaw Excitation Methods

The methods for flaw excitation were also evaluated. No significant changes were noted, either with mechanical probing forces or with broad-area vibration of a possible flawed locality.

9.3.1 Detecting Delaminations by Local Heating

It was theorized that by localized heating and cooling of a suspected flawed area, the exterior surface of the delaminated area would bulge because of local thermal expansion of the matrix or internal pressure generated by vaporized moisture within the delamination. Tests were conducted to evaluate the feasibility of using this effect to increase the apparent size of a defect during Shadow Moire examination.

The following thermal excitation detection procedure was developed and used during the investigation:

- a. The local impact damaged laminate was scanned with the Moire instrumentation to locate the suspected damage site by identifying the local indentation.
- b. Localized heating was applied to the indented area with a hot air gun; to avoid damage, the temperature at the laminate exterior surface was limited to 400°F. The laminate was heated, allowed to cool, and then reheated.
- c. While applying heat, the surface motion in the suspected delaminated area was monitored in the direction normal to the laminate plane.
- d. The heating and cooling cycle was optimized to maximize the out-of-plane bulging movement in the suspected delaminated area.

A small measure of success was achieved with this method of localized thermal excitation. Laminates with implanted TEDLAR patches to simulate flawed localities at various sub-surface levels were subjected to the technique. Out-of-plane surface displacements were detected due to implanted flaws between the 1st and 2nd layers and the 3rd and 4th layers. No out-of-plane surface displacements were detected due to thermal excitation of implanted flaws below the 4th layer. For delaminations of 1/2-inch diameter or greater, the damaged surface bulged. If no delamination or a small insignificant delamination existed, as determined by C-SCAN, no discernible bulging occurred. Figures 24a and 24b show the

NADC-90011-60

Moire fringe patterns generated after heating. The method appears to be promising, but is restricted by the 400°F temperature limitation.

9.4 Digital Image Processing

A preliminary investigation of digital image processing of Moire fringe patterns was investigated during the program. Efforts were directed toward the detection of surface anomalies of .0001 inch or less. The Digital Image Analysis System shown schematically in Figure 25, is able to recognize the light intensity distribution at low order Moire fringe pattern displacement fields using appropriate software, and translate the acquired distribution into fractional fringe orders. The processes of fractional fringe counting and spatial allocation were handled by computer. The observed image and light intensity distribution were recorded with a high resolution video camera and stored on a floppy disc.

The system shown in Figure 26, consisted of the following key components:

- a. 100-watt Tungsten-Halogen Light source.
- b. High Resolution TV Camera, NEC TI22AII
- c. Computer-NEC APC IV - Powermate 1 (IBM-PC-AT Compatible)
- d. Monochrome Monitor - NEC Multisync gs
- e. Data Acquisition Board - 512 x 512 pixels resolution
- f. Coprocessor - for Data Acquisition Board
- g. Color Monitor NEC Multisync II
- h. Printer - Panasonic KX-P1091I
- i. Transparency Table
- j. Operating Software

The operating software consisted of two programs, Fractional Moire Color Analysis (FMCL) and Fractional Moire Line Analysis (FMLA). With this software, an externally generated Moire image is viewed and manipulated with the objective of extracting information by studying picture detail. Computer assisted transformations are applied to isolate and enhance areas of interest within the picture. The analog signal is digitized after input from the video camera. For each frame that is digitized, the database is an array of discrete pixels (picture elements). Within the system, each pixel is a numeric value which represents the intensity of the image at a given point.

A graphite epoxy specimen, (12-inch by 12-inch) was viewed through a 50 lpi Moire screen with the video camera. The image was inputted on the screen of the color monitor and a color representation with a 10X magnification was produced with the FMCL program (Figure 27). A peak

NADC-90011-60

and valley distribution was identified and numbered from left to right with the FMLA program (Figure 28). A printout of the displacement profile is shown in Figure 29. The digital image analysis system can also be adapted to field use with the SMOOPI photographic system (Figure 30). This modification includes a 35mm camera with a extension tube for close-up photography. Negatives can be later processed in the laboratory via the transparency table.

9.5 Additional Applications

The device was used to assess the extent of the cold-work experienced by holes in a metal plate after the hole was expanded and cold-worked with a split sleeve. A fringe was evident at each of the cold-worked holes (Figure 31).

The device was also able to identify minute blisters in an anti-corrosion paint (Figure 32). The blisters cause a breakdown of the corrosion protection and a quick field inspection of the paint was required.

10.0 CONCLUSIONS/RECOMMENDATIONS

Shadow Moire Interferometry has proven to be a simple, quick and effective method of detecting damage in advanced composite structures. It has shown to be effective in locating surface deformations associated with underlying delaminations. Delaminations have been detected both in thin laminates and in the outer plies of thick laminates. The technique has also been very effective in detecting non-visible damage and back-surface shattering due to low-velocity impact.

The test parameters determined using the Moire optical bench, i.e., grid densities and illumination requirements, were used to design and fabricate a prototype model of the Shadow Moire Out-of-Plane Interferometric (SMOOPI) Damage Detector. This instrument has proved successful in field-like inspections. The SMOOPI Damage Detector has several advantages over existing Non-Destructive Inspection techniques. It is an accurate, reliable, portable, lightweight, low-cost device that can be used in the field by personnel with minimum training and eliminates the tedious scanning procedures required to inspect large structures. Flaw sites can be identified quickly; then ultrasonics (A-SCAN or C-SCAN) can be used at selected flaw locations to further quantify flaw extent, if necessary.

The SMOOPI Damage Detector permits the use of high-density grids (up to 1000 lpi) because of the minimal clearance and three-point contact system for curved surfaces. An attached heat gun can also be employed as an excitation force for detecting delamination.

Mechanical probing and broad-area sonic vibrations were deemed ineffective in extending the damage-detection capability of the Moire instrumentation via flaw enhancement. Localized heating, on the other hand, met with some measure of success, limited only by the temperature restriction to 400°F. The Grid-Bias Linear Carrier-Fringe Method showed itself to be a more promising technique for sensitivity enhancement.

NADC-90011-60

A preliminary investigation of the digital image processing technique indicated that it may be possible to produce a 10X magnification of the Moire signal. This process shows a potential for future development, but because of size and weight limitations, may not be adaptable to field use. It may be possible, however, to adapt to a field application with a Photographic or Camcorder System, and data can be later processed in the laboratory.

10.1 Transition

The SMOOPI device developed and built at the Naval Air Development Center has been demonstrated at the Naval Air Systems Command (NAVAIR) and several Naval Air Depots and received a favorable response. The Navy's maintenance community has expressed enthusiastic interest and Naval Air Depots at Norfolk, Virginia, and Cherry Point, North Carolina, and Alameda, California are further exploring the operational procedures of the device under actual field conditions. The U.S. Air Force has also expressed an interest in using the device and demonstrations are planned at Wright-Paterson, McClellan, and Tinker Air Force Bases. The device is being used to assist Lehigh University with a National Science Foundation grant to detect defects and blisters in anti-corrosion paints. It was also successful in detecting cold-worked holes in metal specimens supplied by Fatigue Technology Incorporated. Major aerospace companies: Grumman, Boeing, General Dynamics, Lockheed, Rohr Industries, and Aerobond Inc., are interested in using the device. McDonnell Douglas plans to use it in conjunction with their own development, the Mobile Automated Ultrasonic System. Meetings and demonstrations are in progress. The Israel Air Force and the Defense Research Center Pacific, Victoria, B.C. would also like to evaluate the damage detector and have been sent several reports. The Swiss Federal Aircraft factory would like to purchase the device and have requested a quotation. A patent application has been filed and an exclusive license for the commercial development of the device is being negotiated.

The SMOOPI Damage Detector Kit, shown in Figure 14, has been sent to several Naval Depots at their request. An instruction manual "Description, Principles and Applications of the SMOOPI Damage Detector" by A. E. Scotese, has also been provided. The commercial version of the device and kit is now being finalized. Additional accessories, e.g., camera, telemicroscope, zoom lens, extension tube and mounting brackets will also be available. Further research relative to quantification of Moire cold-work detection has been requested by NAVAIR and a Statement of Work is being provided.

REFERENCES

1. Fanucci, J. P. and Mar, J. W., "Fatigue Damage Detection in Thin Composites Laminates Using Out-of-Plane Moire Interferometry," Department of Aeronautics and Astronautics, M.I.T. Cambridge, MA 02139, 1982.
2. Nevadunsky, J. J., Lucas, J. J. and Salkind, M. J., "Early Fatigue Damage Detection in Composite Materials," Vol. 9, October 1975, pp. 394-407.
3. Fanucci, J. P., "Damage Initiation and Propagation During Compressive Fatigue of Flawed Graphite/Epoxy Composites," Doctoral Thesis, Massachusetts Institute of Technology, Department of Aeronautics and Astronautics, September 1980.
4. Hahn, H. T. and Kim, R. Y., "Fatigue Behavior of Composite Laminates," Journal of Composite Materials, Vol. 10, April 1976, pp. 156-180.
5. Reifsnider, K. L., Hennecke, E. G. II, and Stincomb, W. W. "Delamination in Quasi-Isotropic Graphite-Epoxy Laminates," ASTM STP 617, 1977, pp. 93-105.
6. Rhodes, Marvin D., Williams, Jerry G. and Starnes, James H., "Effect of Low Velocity Impact Damage on the Compressive Strength of Graphite/Epoxy Hat-Stiffened Panels," NASA Technical Memorandum NASA TM X-73988, December 10, 1976.
7. Chang, F. H., Gordon, D. E. and A. H. Gardner, "A Study of Fatigue Damage in Composites by Nondestructive Testing Techniques," ASTM STP 636, K. L. Reifsnider and K. N. Lauritis, (eds.), 1977, pp.57-72.
8. Vary, A., "A Review of Issues and Strategies in Nondestructive Evaluation of Fiber Reinforced Structural Composites," Proceedings 11th National SAMPE Technical Conference, November 1979, pp. 178-191.
9. Durelli, A. J. and Parks, V. J., "Moire Analysis of Strain", Prentice-Hall, Inc, Englewood Cliffs, NJ, 1970.
10. Theocaris P. S., " Moire Fringes in Strain Analysis, "Pergamon Press, New York, 19111 1969.
11. Post, D. "Developments in Moire Interferometry," Optical Engineering Vol. 21, No. 3, June 1983, pp. 458-467.
12. Basehore, E. M. and Post D., "Moire Method for In-Plane and Out-of-Plane Displacements", Experimental Mechanics, Vol. 21, No. 9, September 1981, pp. 321-328.
13. Chiang, Fu-Pen, "Moire Methods of Strain Analysis", Chapter VI, Manual on Experimental Stress Analysis, Published by the Society Experimental Mechanics, 1986.

NADC-90011-60

14. Post, D., "Moire Interferometry for Damage Analysis of Composites," Experimental Techniques, Vol. 7, No. 7, July 1983.
15. Post, D., "Optical Interference for Deformation Measurements - Classical, Holographic and Moire Interferometry," Mechanics of Non-Destructive Testing, (ed.) W. W. Stinchcomb, Plenum Publishing Corp., NY, 1980
16. O'Brien, T. K., "Characterization of Delamination Onset in a Composite Laminate," Damage in Composite Materials, 775, K. L. Reifsnider, E., American Society for Testing and Materials and Testing, pp. 103-117.
17. Knauss, W. G., Babcock, C. D. and Chai, H., "Visualization of Impact Damage of Composite Plates by Means of the Moire Technique," NASA Contractor Report 159261, April 1980.

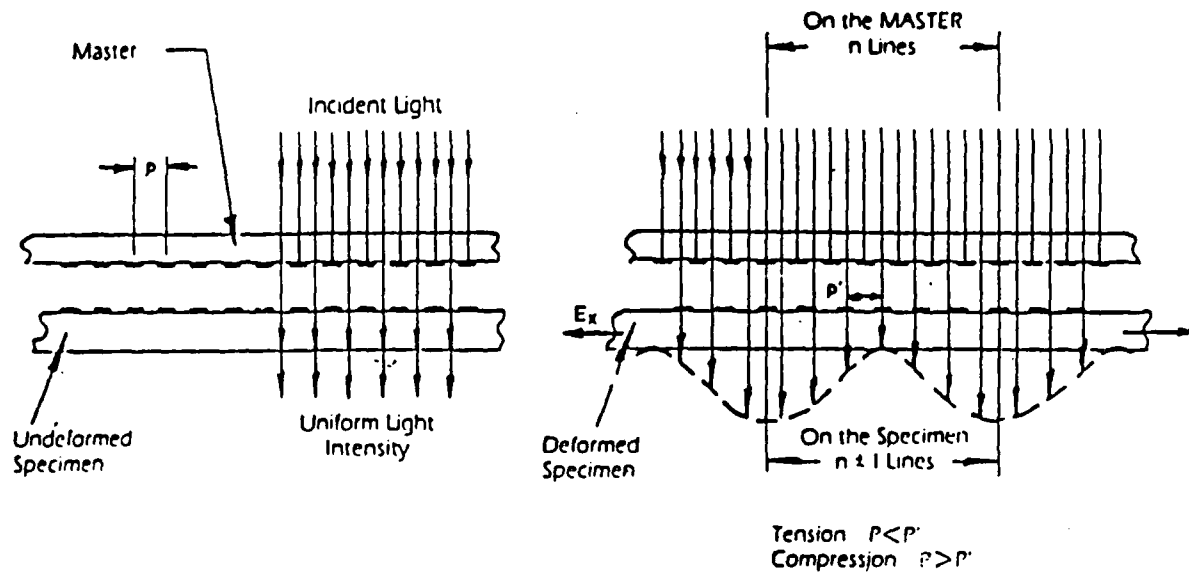


Figure 1. Moire Fringe Analysis: Superposition of Master and Specimen Grids

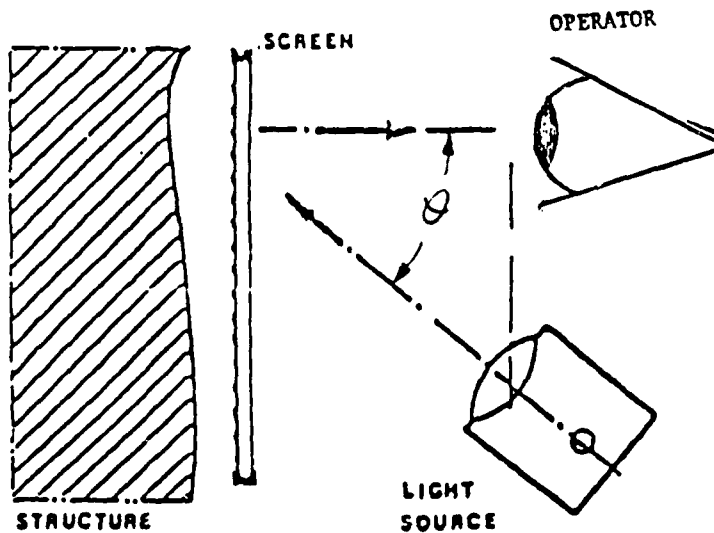


Figure 2. Shadow Moire: Schematic Diagram of Setup

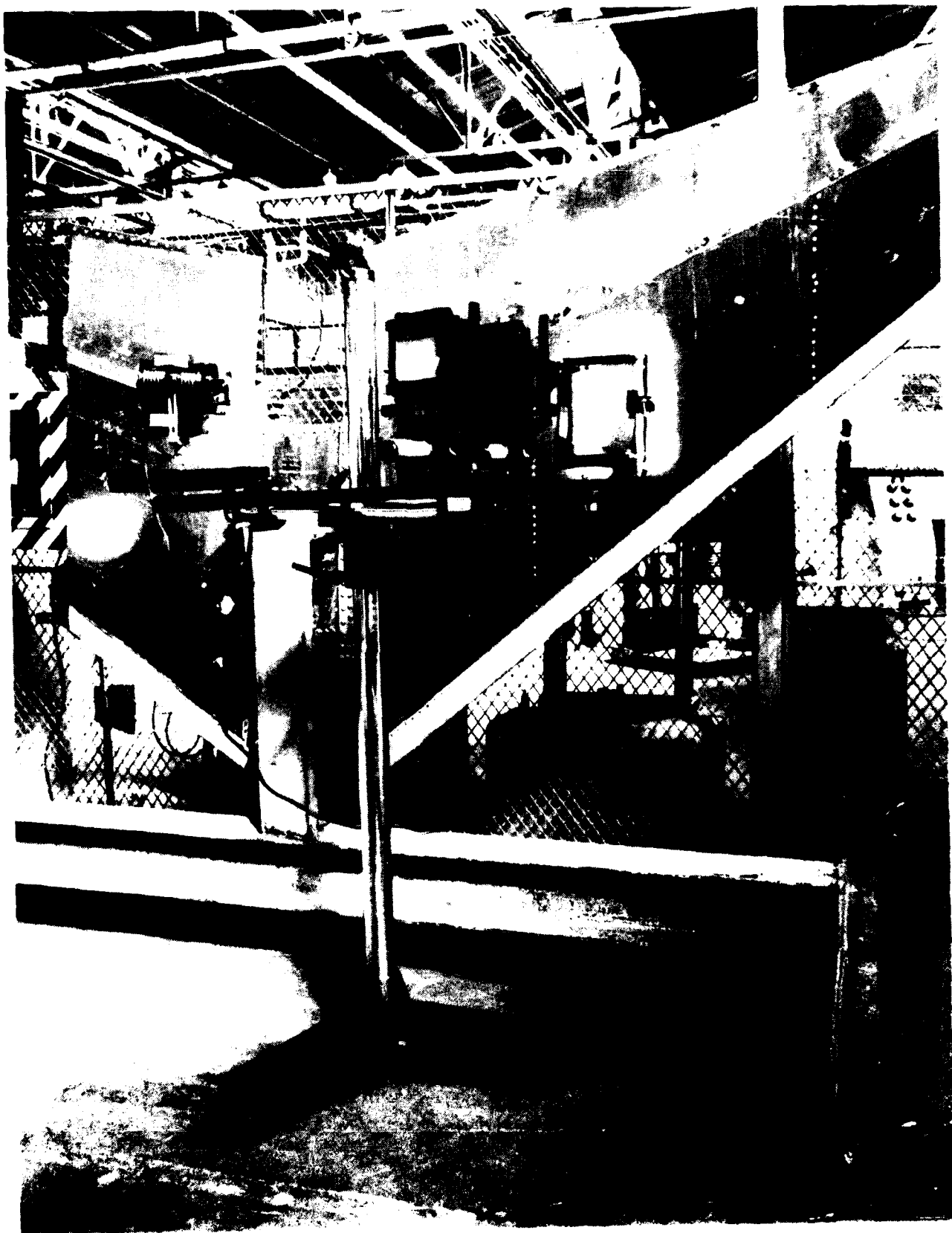


Figure 3. Portable Shadow Moiré Optical Bench

NADC-90011-60

TABLE 1 DISPLACEMENT PER FRINGE FOR SMOOPI DAMAGE DETECTOR

ANGLE OF INCIDENCE DEGREES	GRID LINE DENSITY LPI	50	150	250
30		.0345	.0118	.0069
45		.020	.0067	.004
63.5		.010	.0033	.002
75		.0034	.0018	.0011

NADC-90011-60

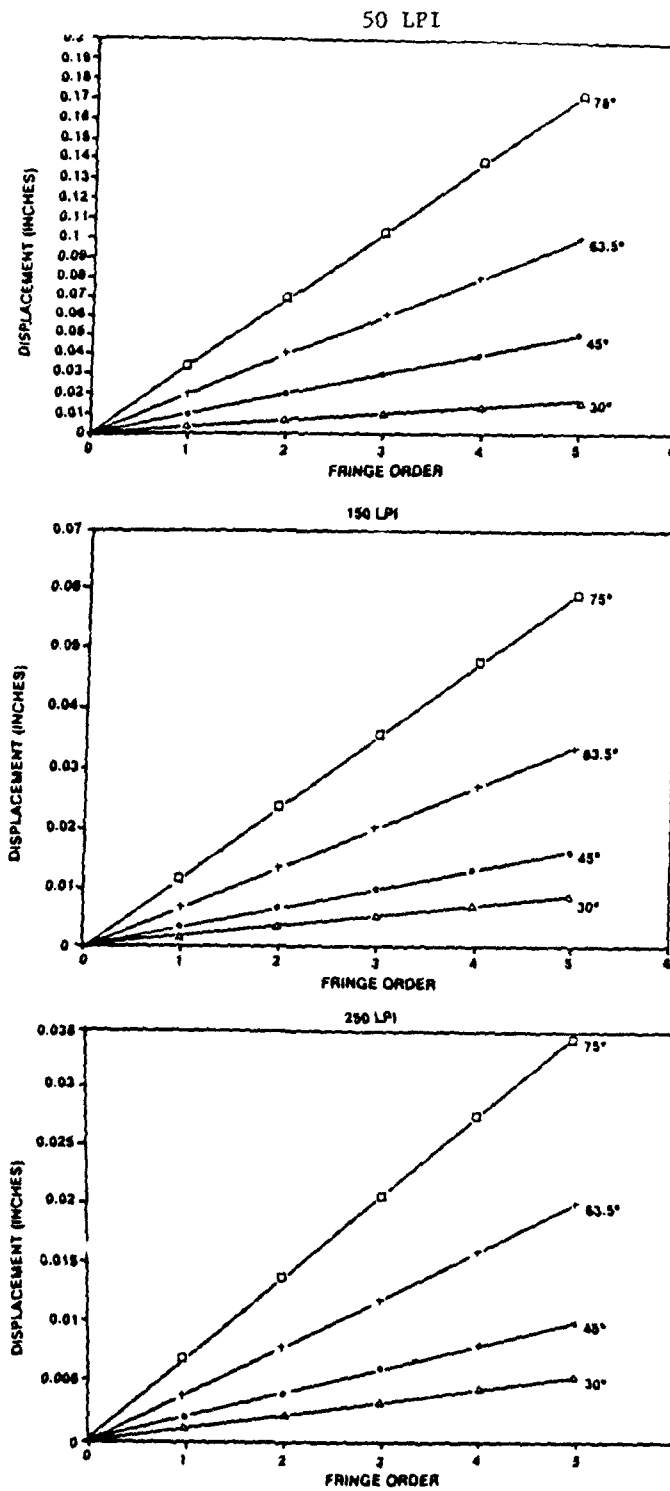


Figure 4. Displacement Per Fringe for SMOOPI Damage Detector



Figure 5. Moire Fringes (3) About Lower Hole, After Fatigue Cycling, Inspected with 500 lpi Grid: 25 Ply GR/EP Specimen; Out of-Plane Displacement 0.003 Inch

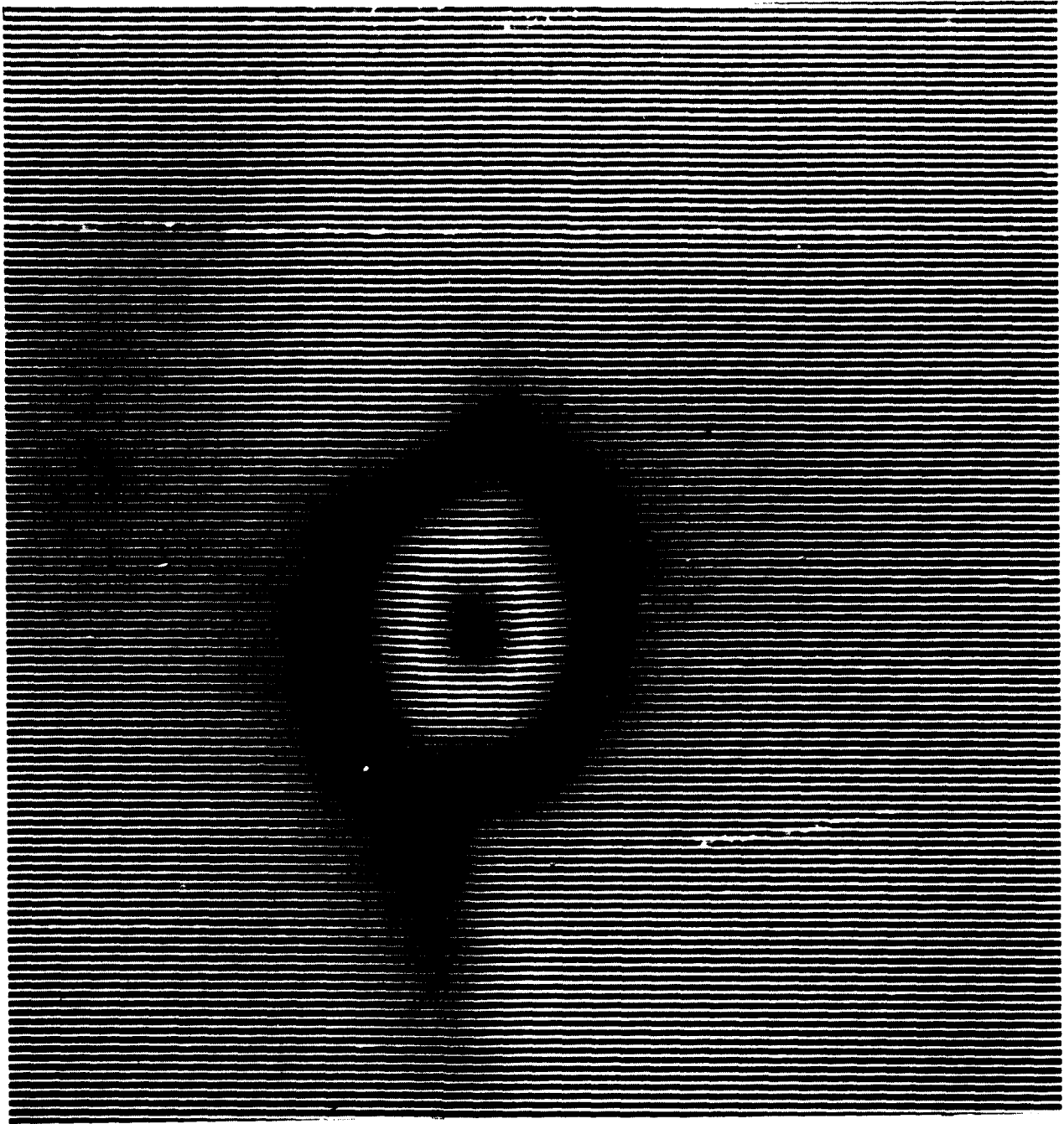


Figure 6. Moire Fringes (2), After Impact Testing 40 Ply GR/EP Specimen, 0.02 Inch Out-of-Plane Displacement

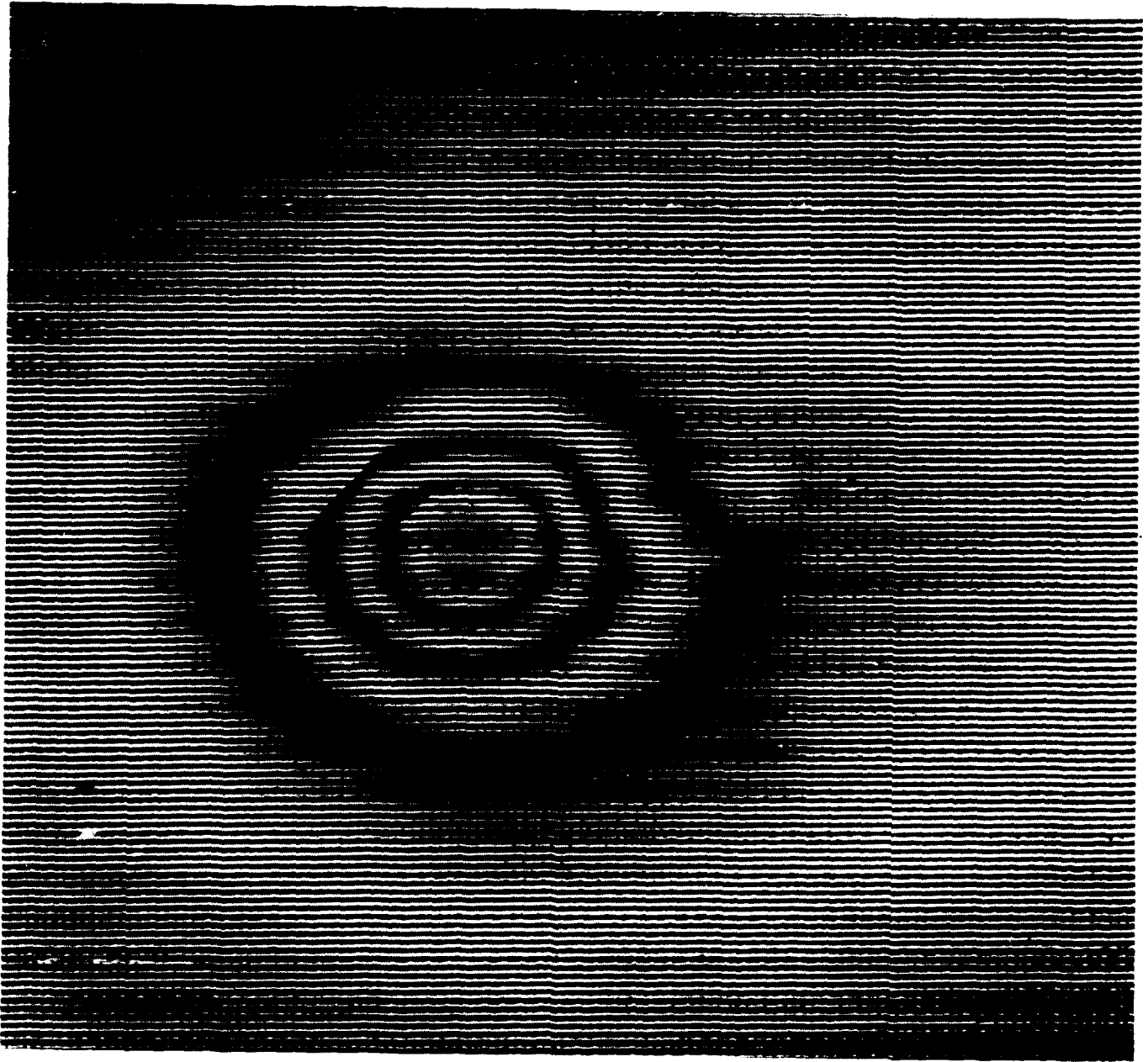


Figure 7. Moire Fringes (4), After Impact Testing; 40 Ply
GR/EP Specimen, 0.04 Inch Out-Of-Plane Displacement



Figure 8. SMOOPI Portable Damage Detector Being Used to Inspect AV-8B Stabilator for Impact Damage

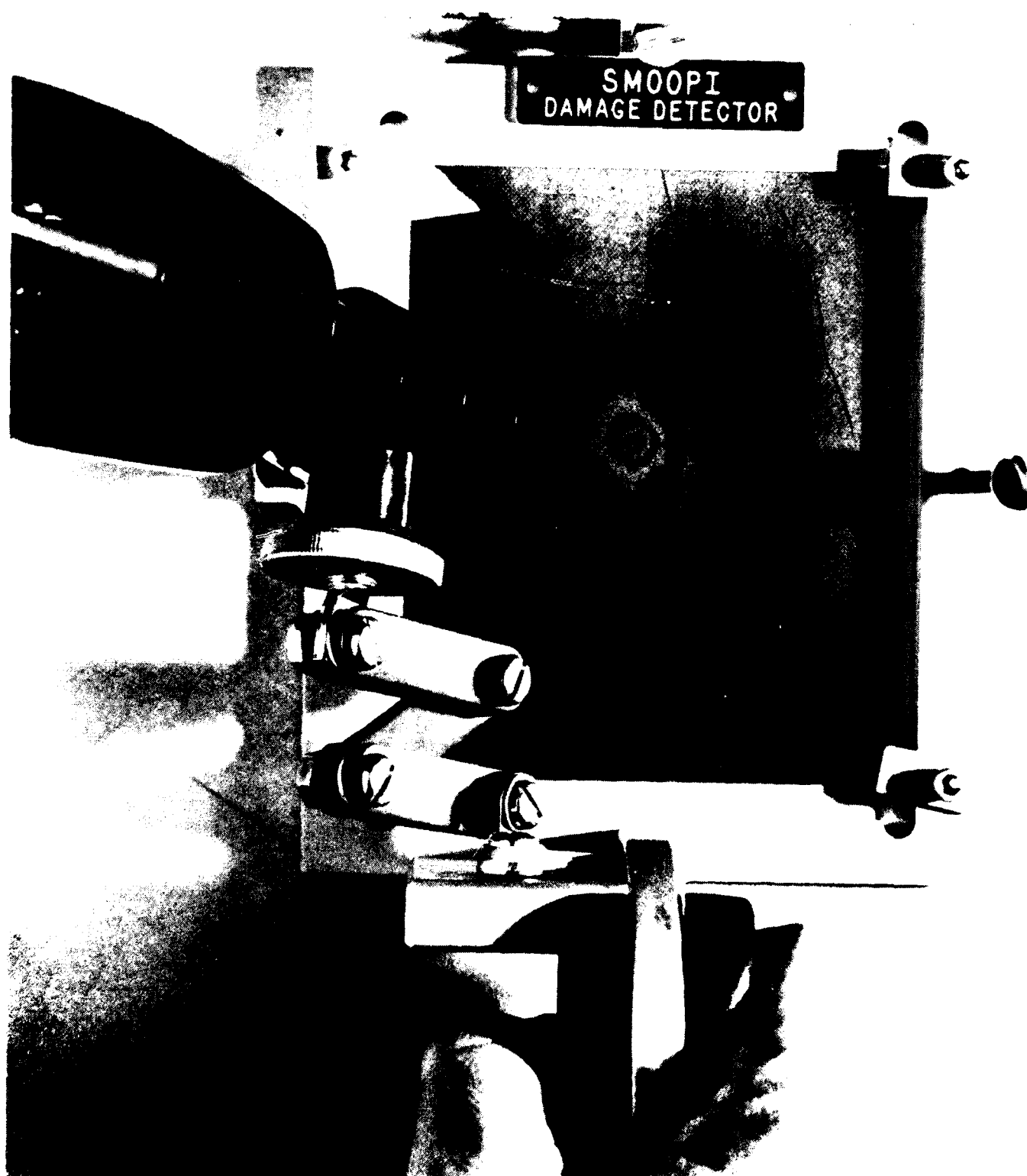


Figure 9. SMOOPI Damage Detector Showing Non-Visible Impact
Damage: 0.004 Inch Displacement

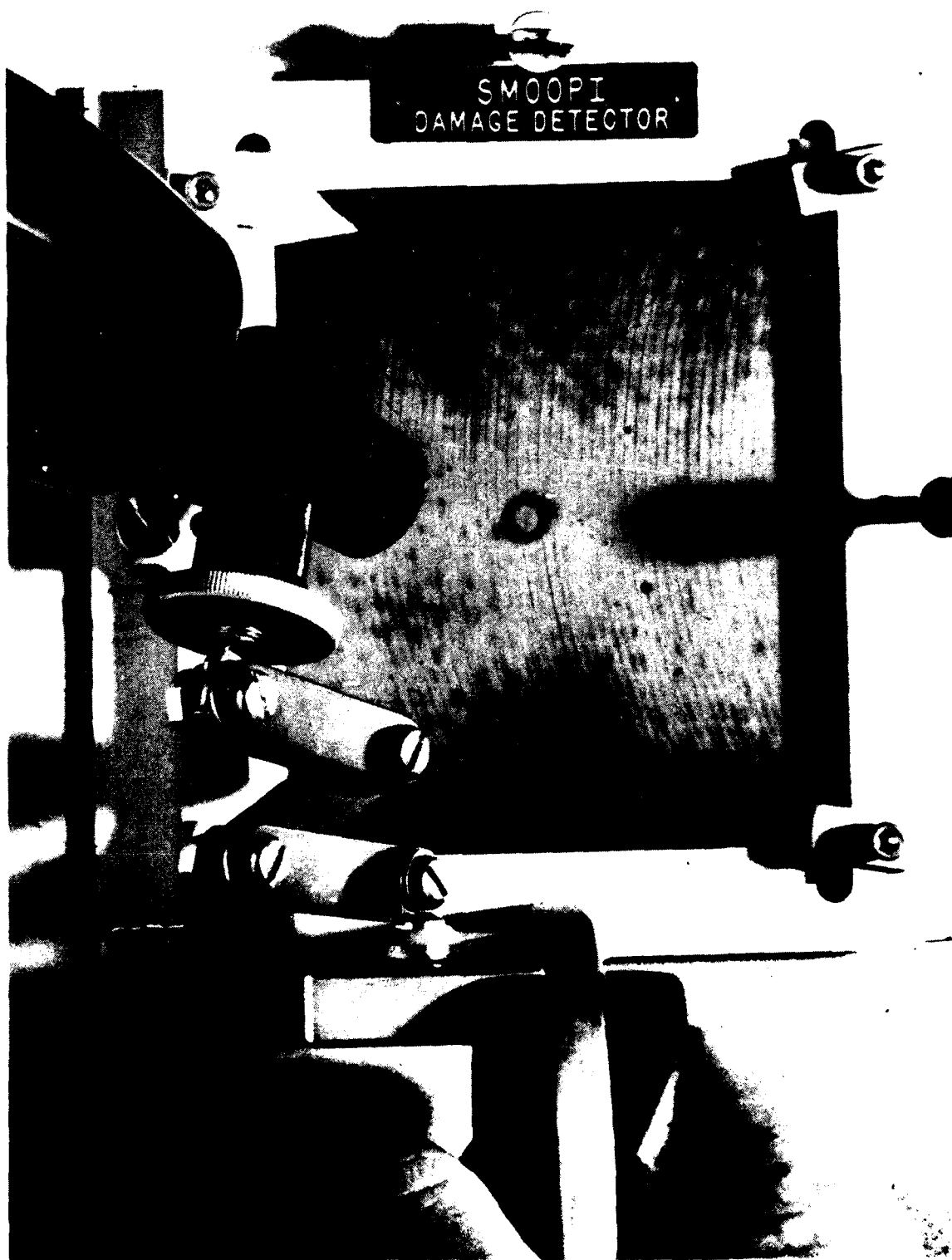


Figure 10. SMOOPI Damage Detector Showing Non-Visible Impact
Damage: 0.001 Inch Displacement



Figure 11. Photomicrographs (100X) of 40 Ply GR/EP Specimen
After Impact Damage, Note Delaminations

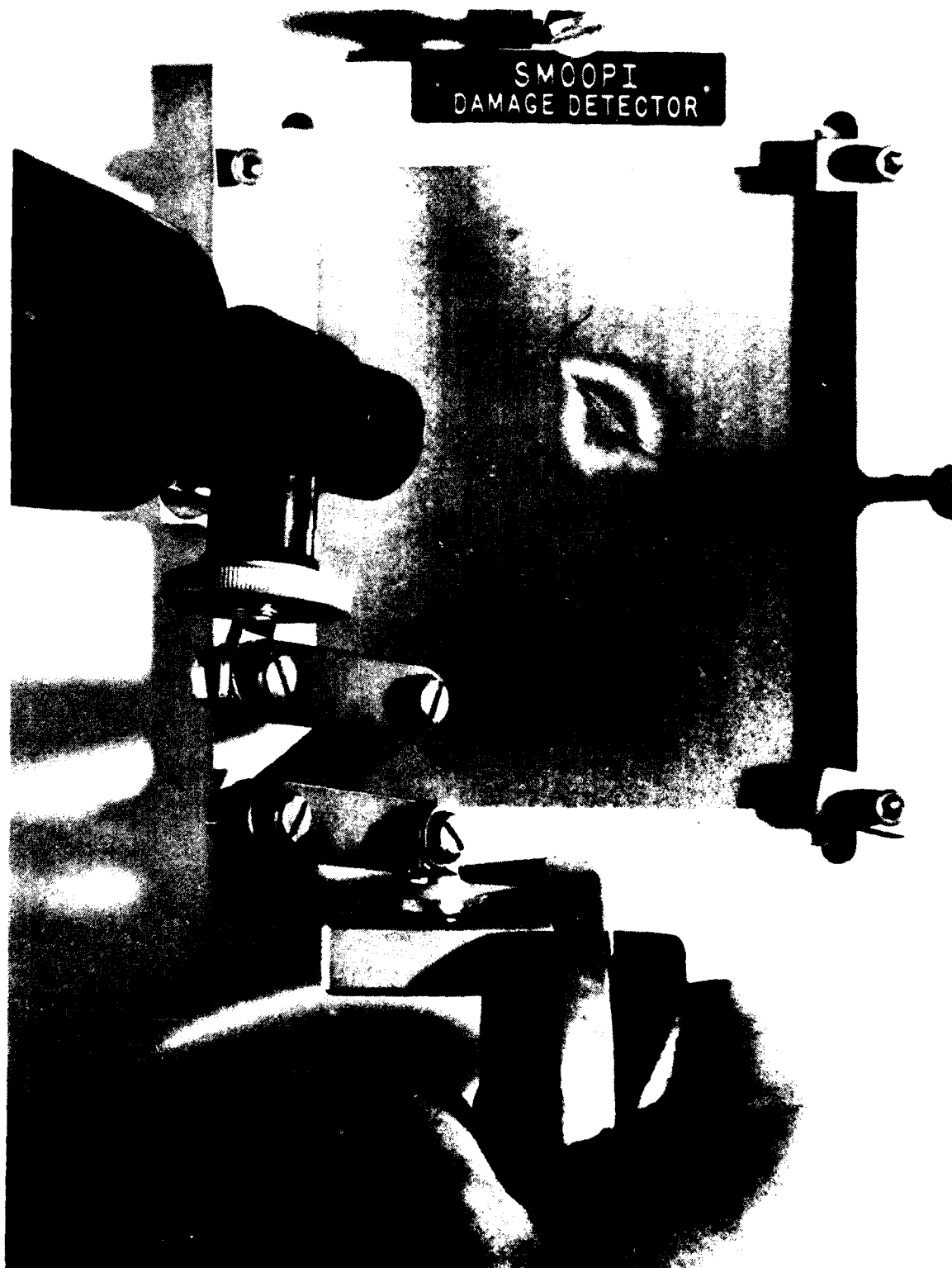


Figure 12. SMOOPI Damage Detector Showing Out-Of-Plane Displacement of Top Surface Resulting from Back-Surface Shattering

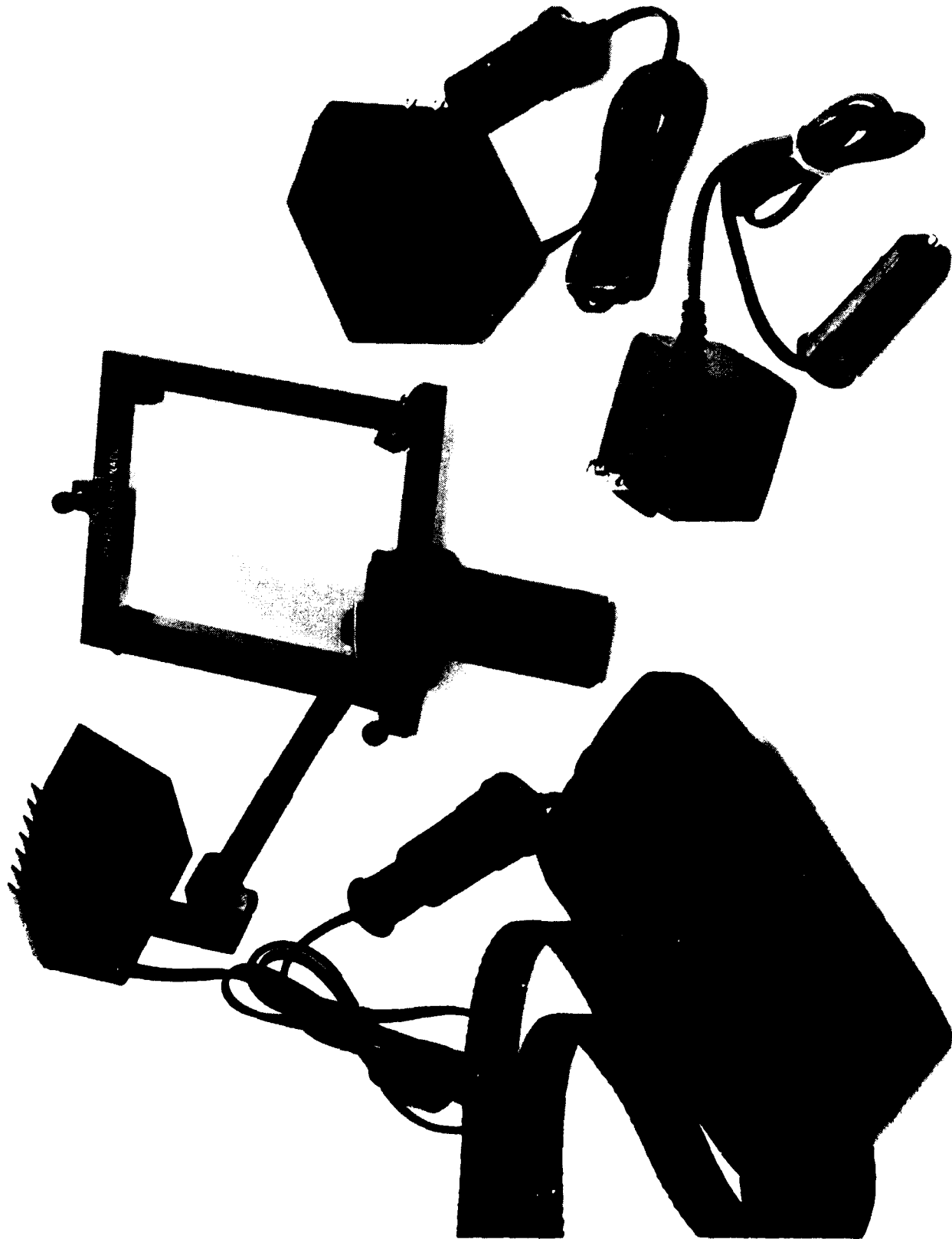


Figure 13. Shadow Moire Out-Of-Plane Interferometric (SMOOP) Damage Detector with Battery-Pack, Charger & AC Adapter

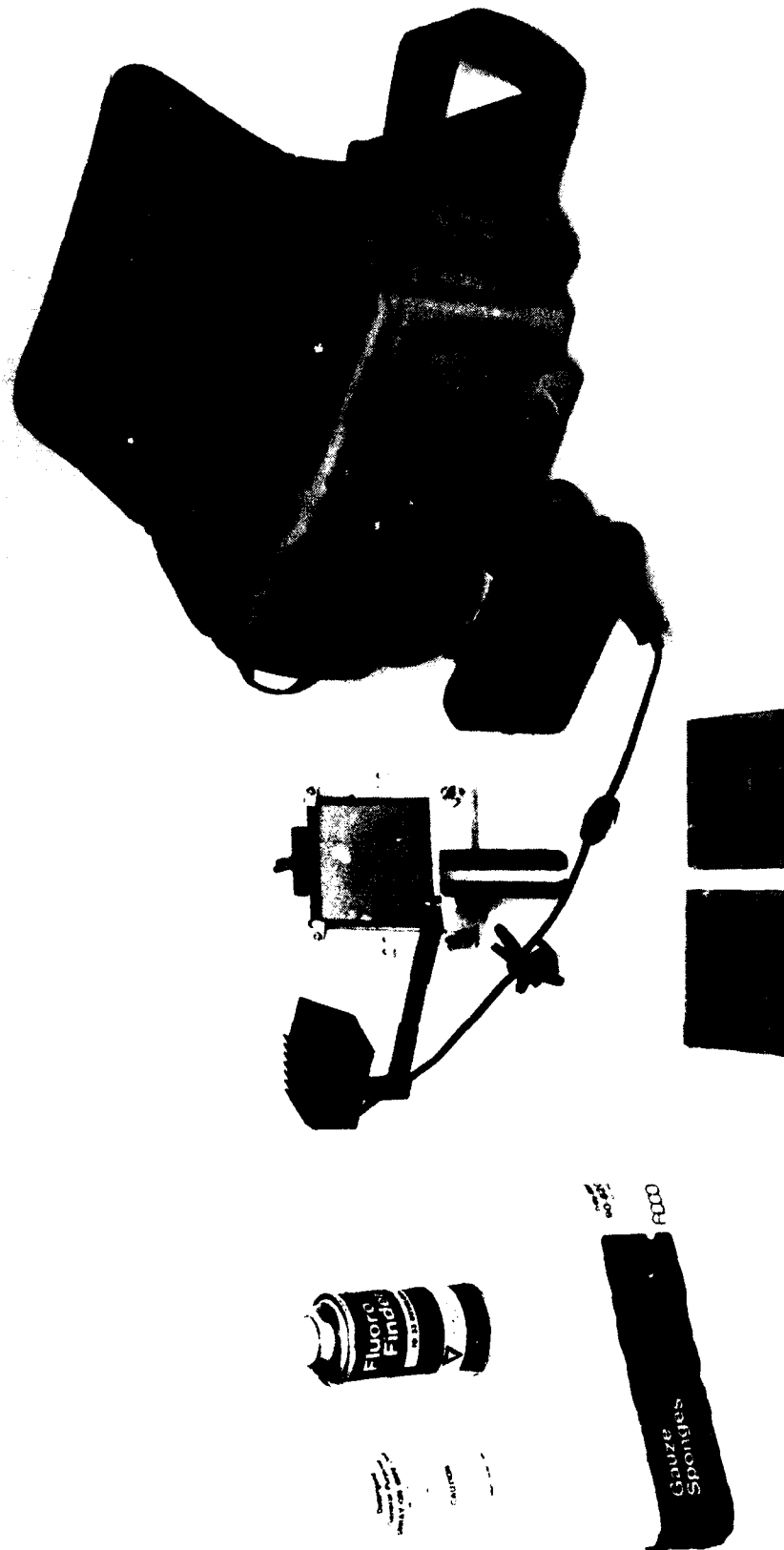


Figure 14. SMOOPI Damage Detector Kit

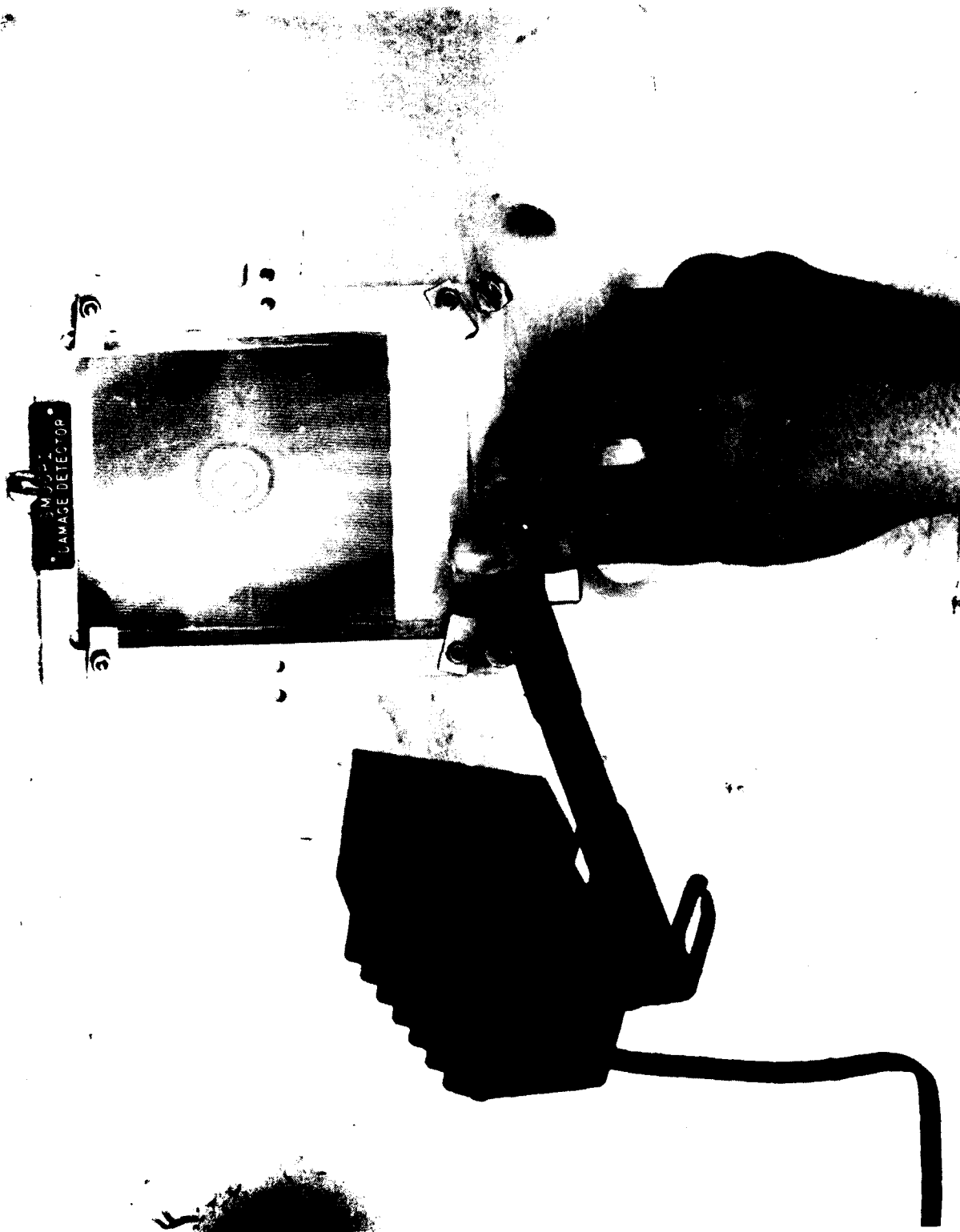


Figure 15. Spherically Shaped Impact Damage, Three Fringes, .01 Inch Per Fringe Displacement, 50 Ipi Grid, 63.5° Incidence Angle

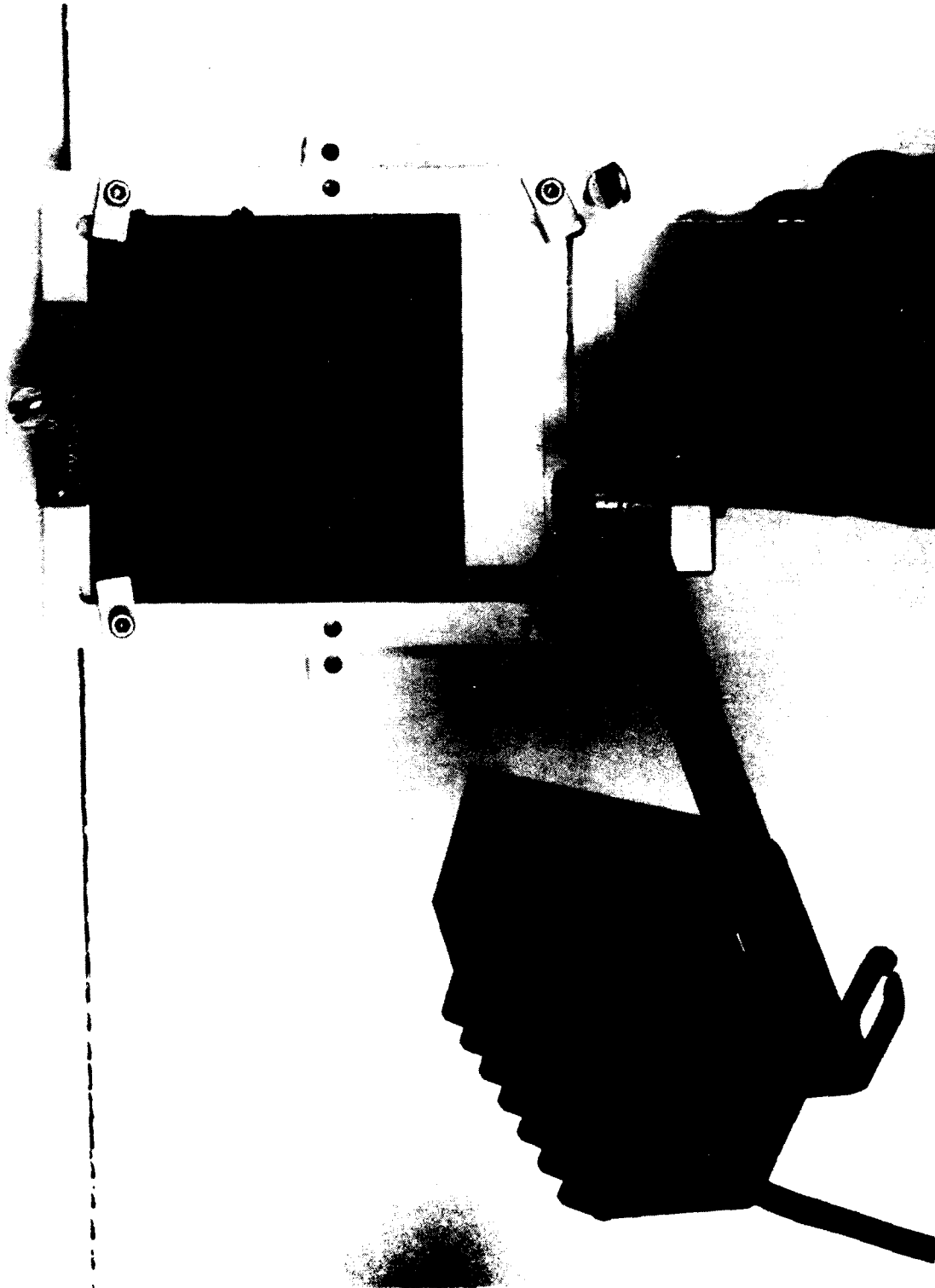


Figure 16. Three Fringes - Elliptically Shaped Surface Contours, 150 lpi Grid, 45° Incidence Angle, .0067 Inch Per Fringe Displacement, Viewed After Impact

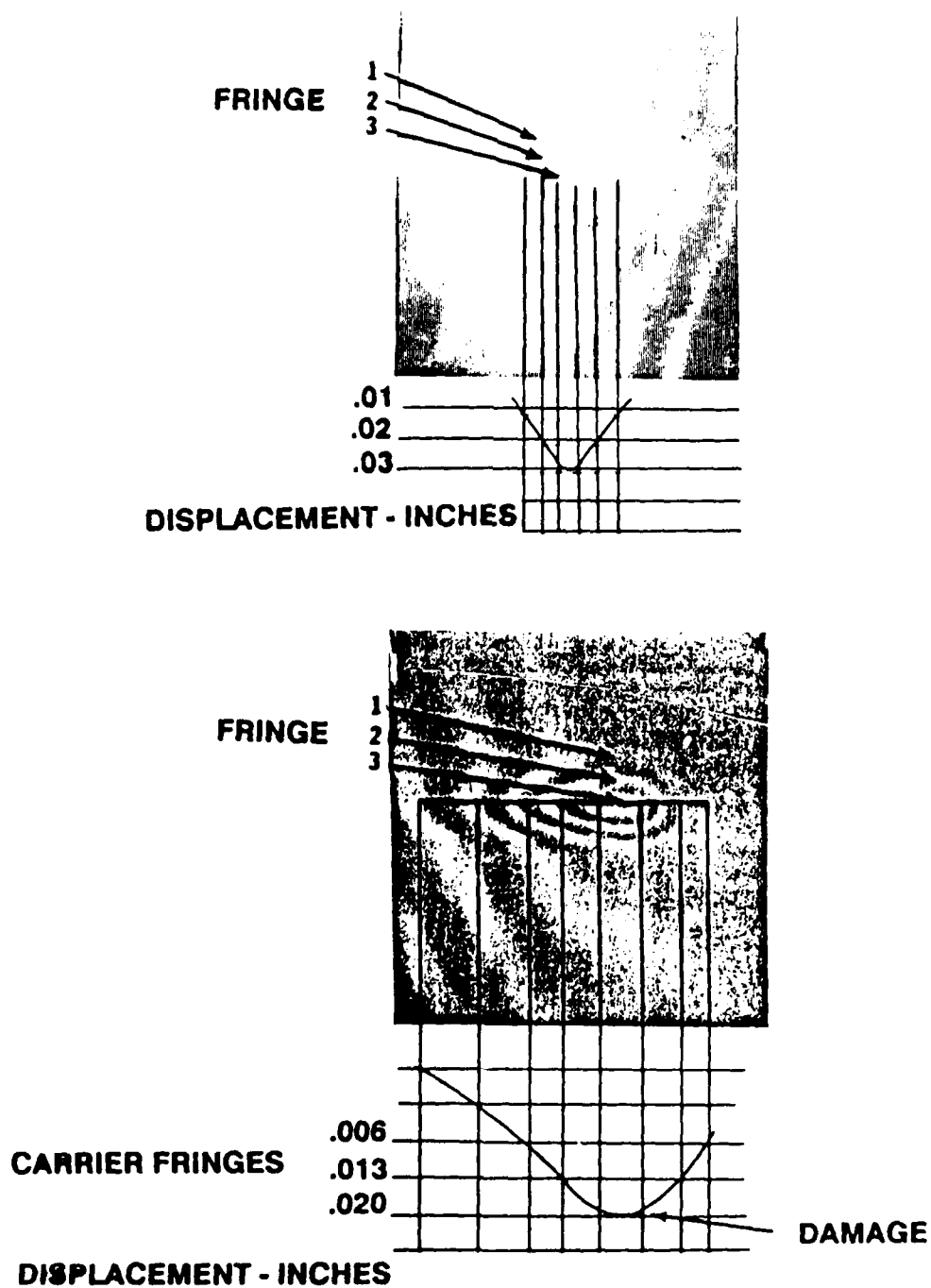


Figure 17. Damage Displacement Profiles

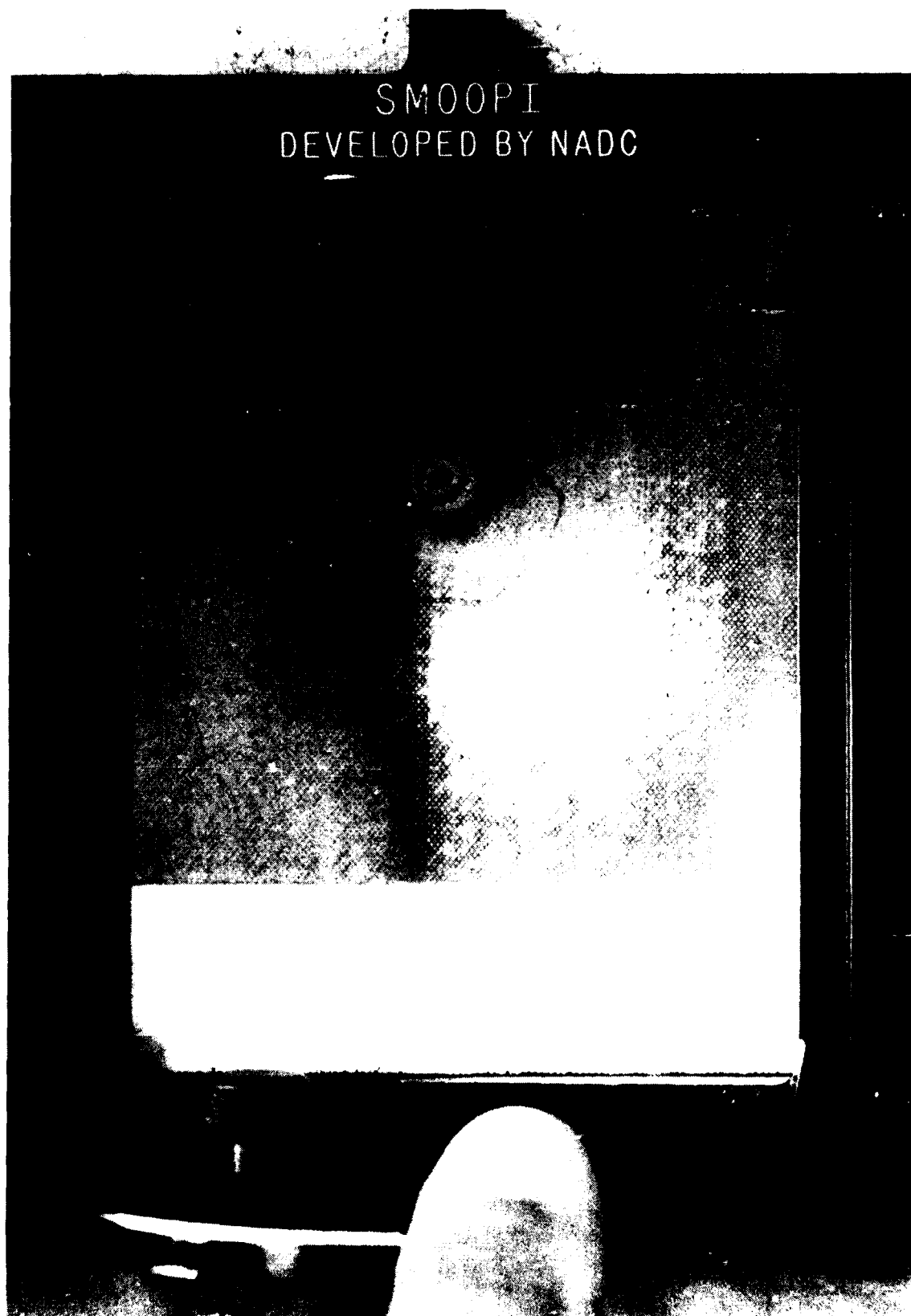


Figure 18. Three Fringes - 250 lpi Grid, 63.5° Incidence Angle, .002 Inch Per Fringe Displacement, Viewed After Impact

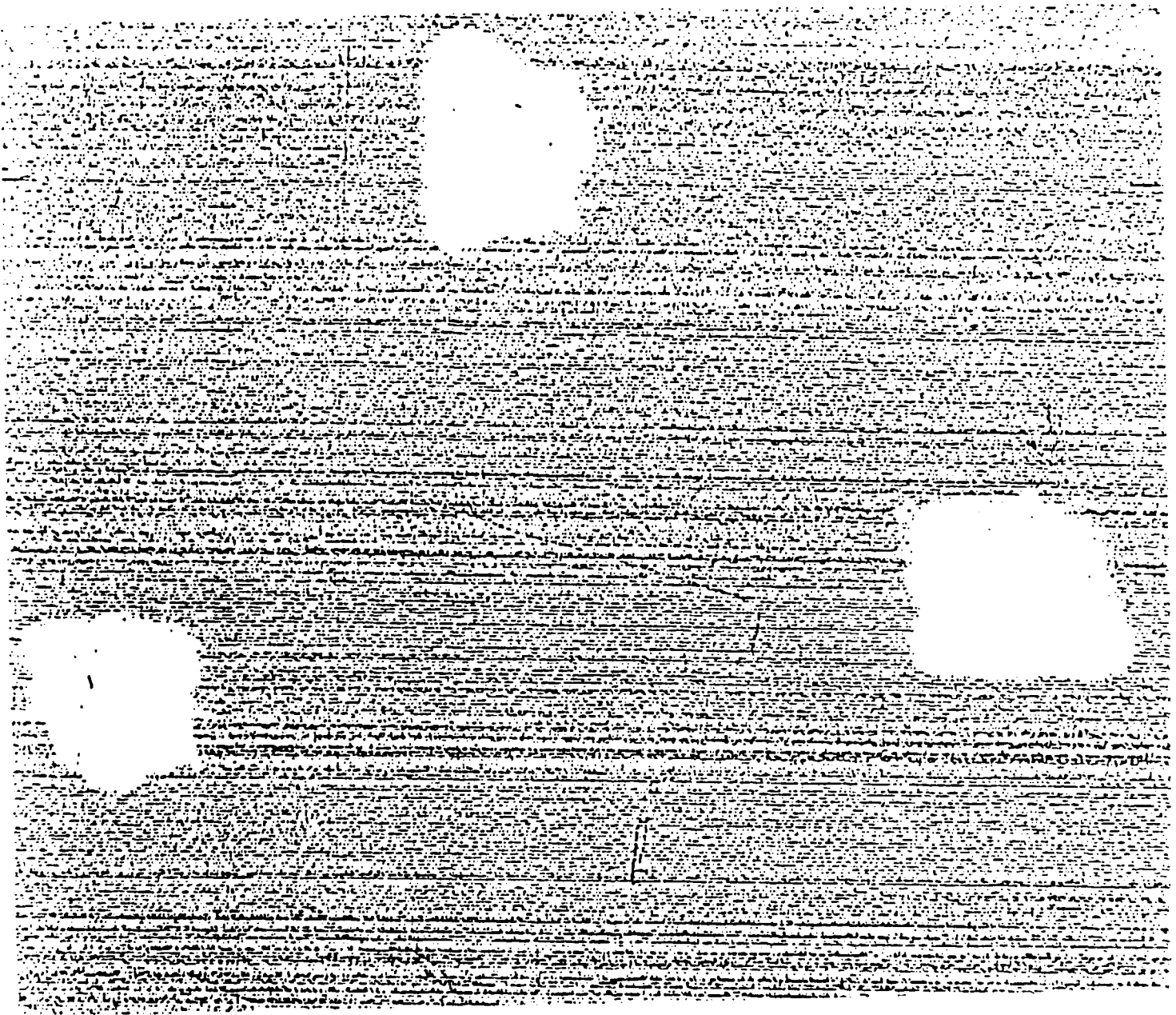


Figure 19. Ultrasonic C-Scan of Specimen in Figure 18



Figure 20. Grid-Bias Linear Carrier Fringes: Moire Fringes With Out-Of-Plane Grid Rotation to Increase Sensitivity, After Impact; 50 Ply GR/EP Specimen

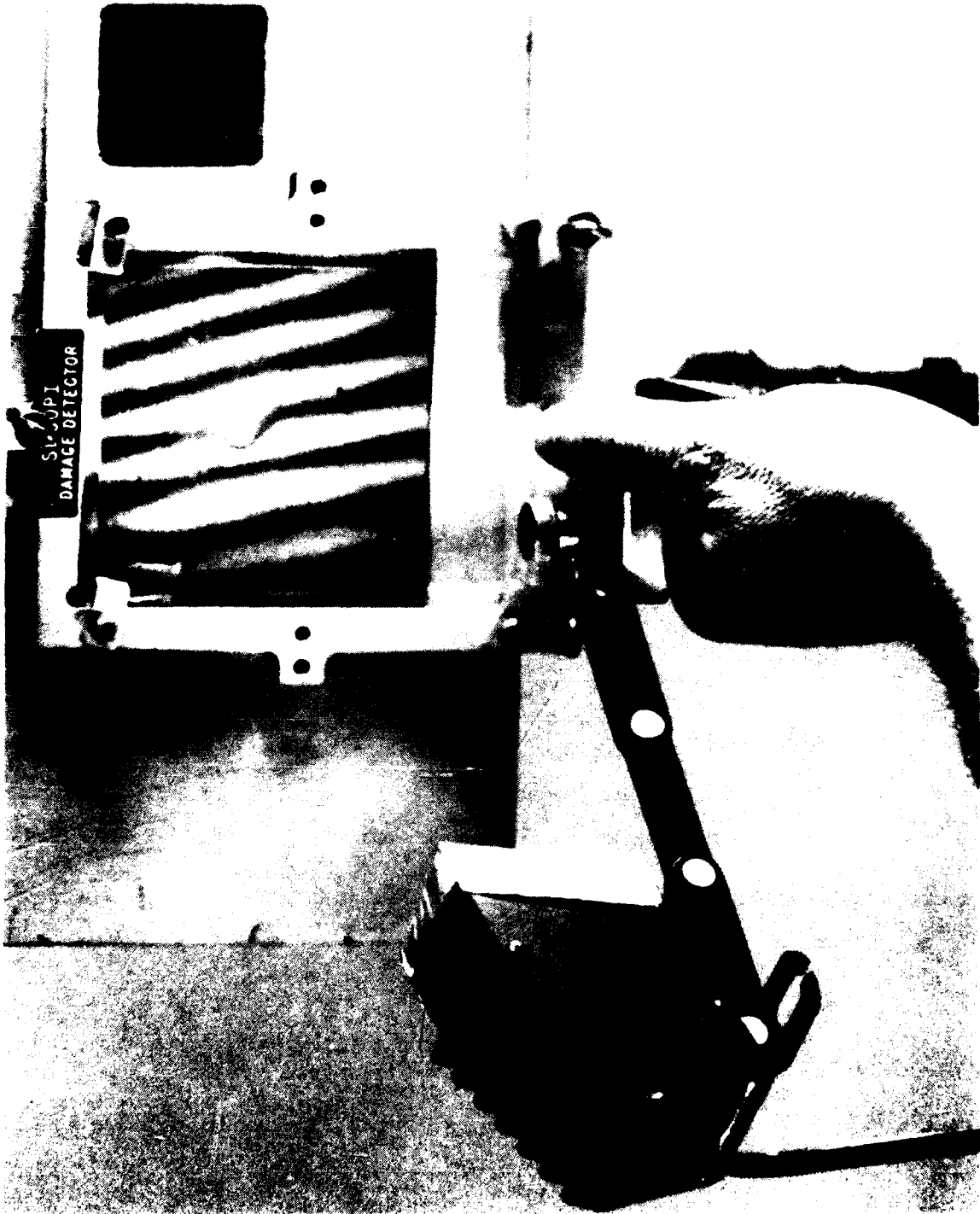


Figure 21. Carrier Fringes - 1 1/2 Fringe Order (out-of-line movement at center)
150 lpi Grid, 45° Angle of Incidence

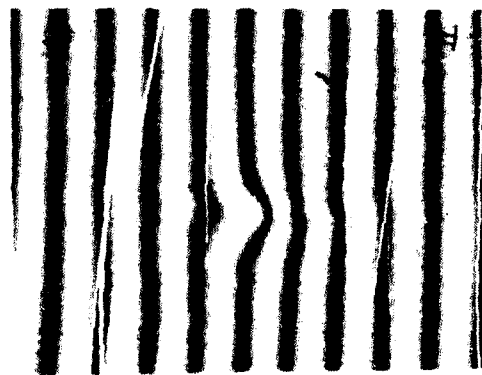
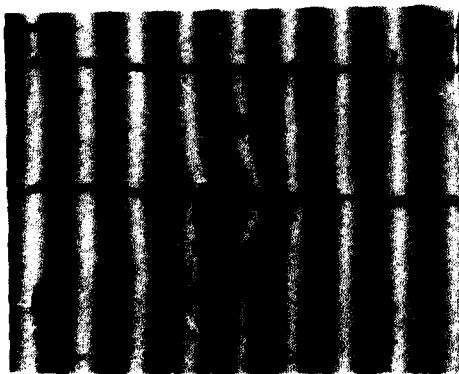
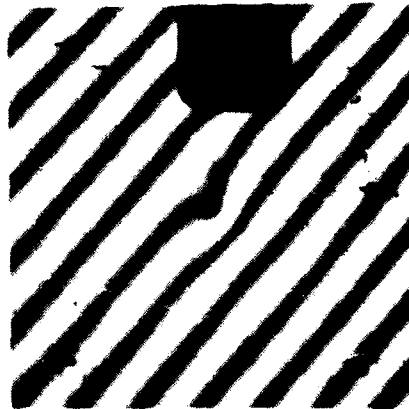


Figure 22. Grid-bias Linear Carrier Fringes; 40 Ply GR/EP
Specimen Viewed After Impact. 250 lpi Grid, 63.5°
Angle of Incidence. Visual Sensitivity for 1/4 Fringe
Interpolation Equals .0005

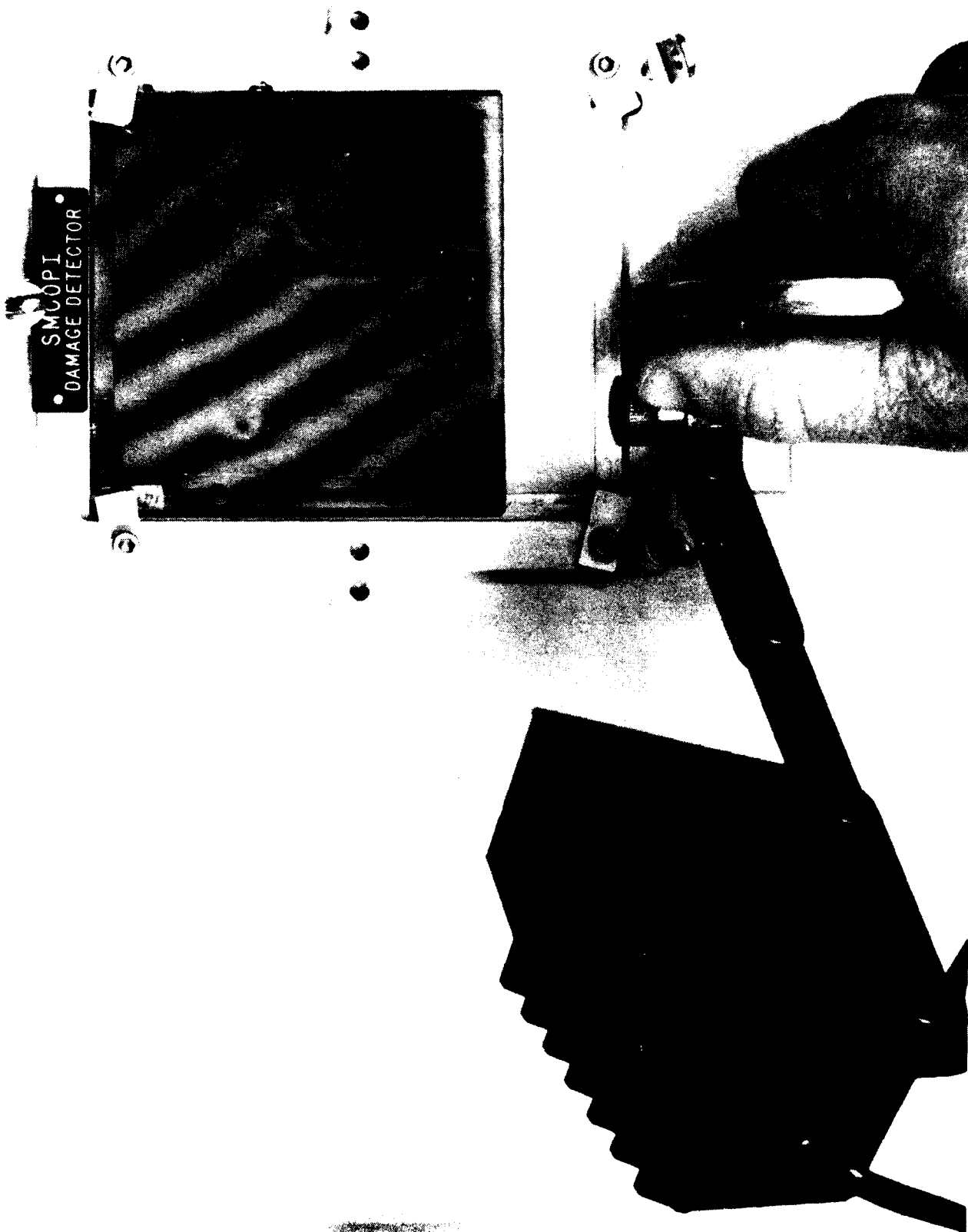
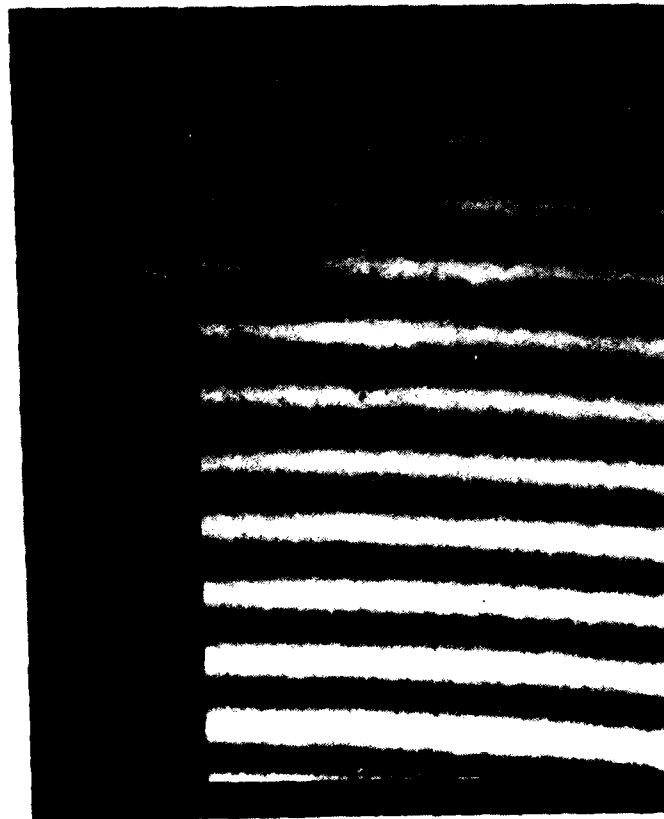


Figure 23. Low and High Order Displacement Area - $1+1/2$ and 4 Fringes, 150 lpi Grid, 63.5° Incidence Angle, .0033 Inch Per Fringe Displacement

NADC-90011-60



A



B

Figure 24. Moiré Fringes Generated After 400°F Heat Excitation of Suspected Flaw Area

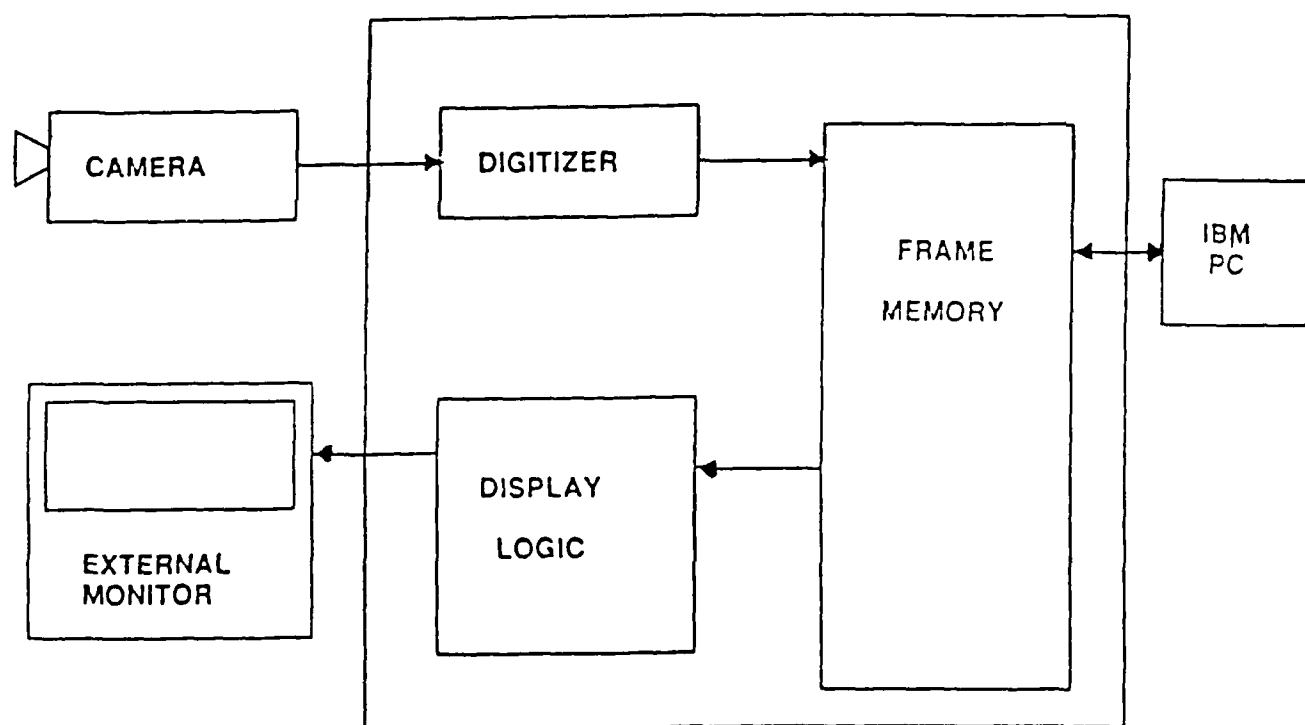


Figure 25. Computerization System



Figure 26. Digital Image Processing System



Figure 27. Color Program for 10X Resolution Enhancement for Digital Image Processing

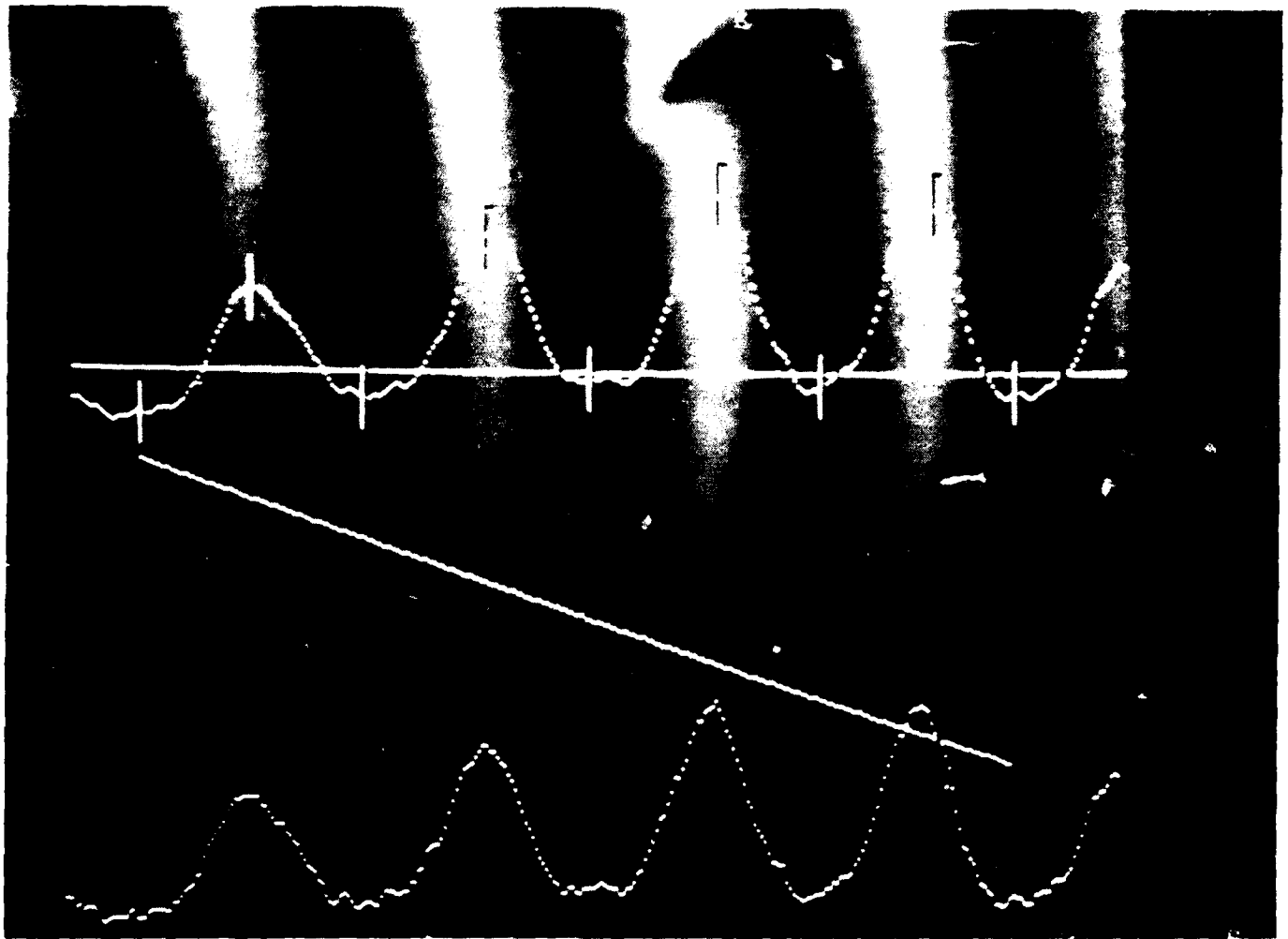


Figure 28. Digital Image Processing - Line Program for
Determination of Out-Of-Plane Deformation Profile

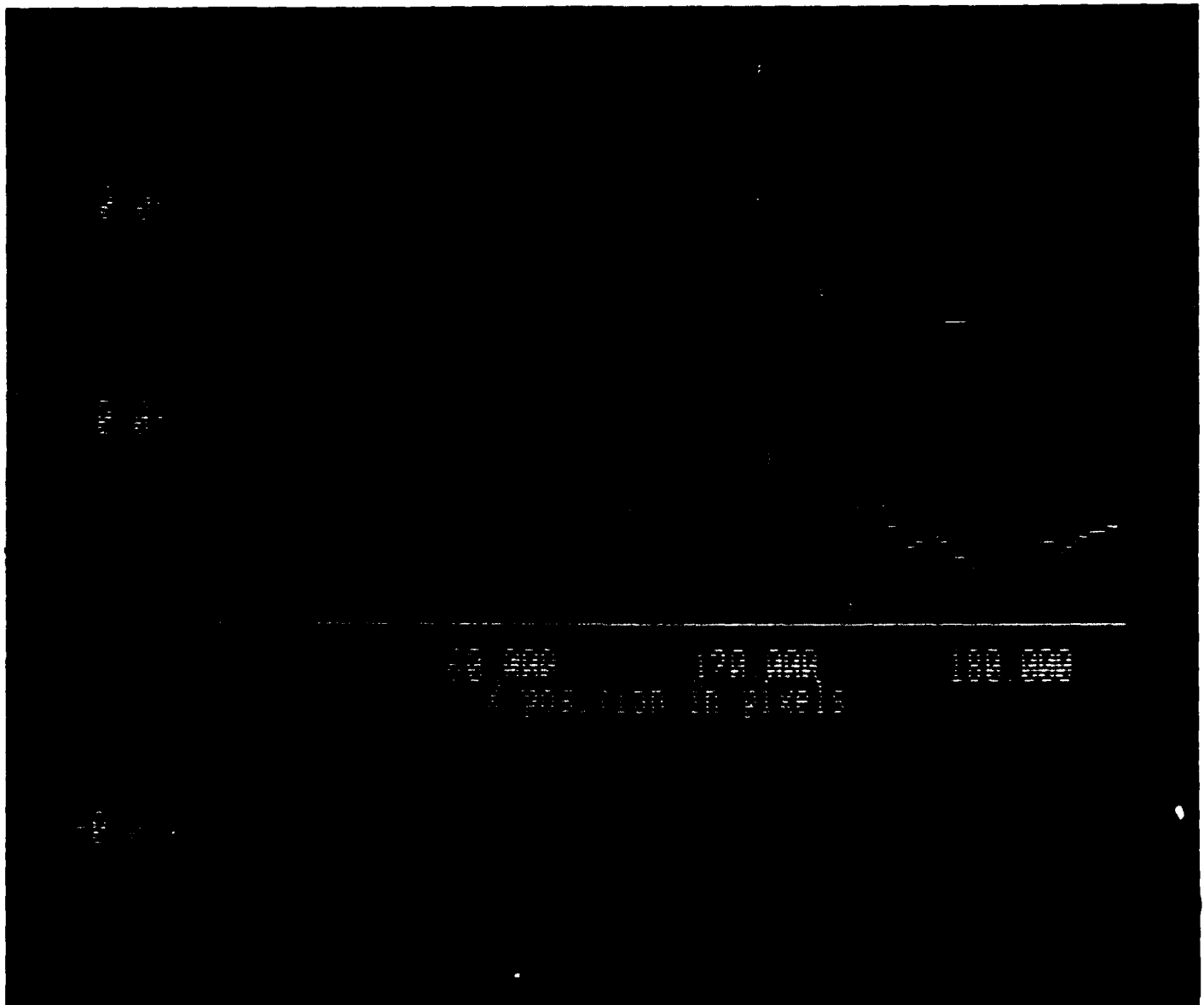


Figure 29. Displacement Profile (inches)

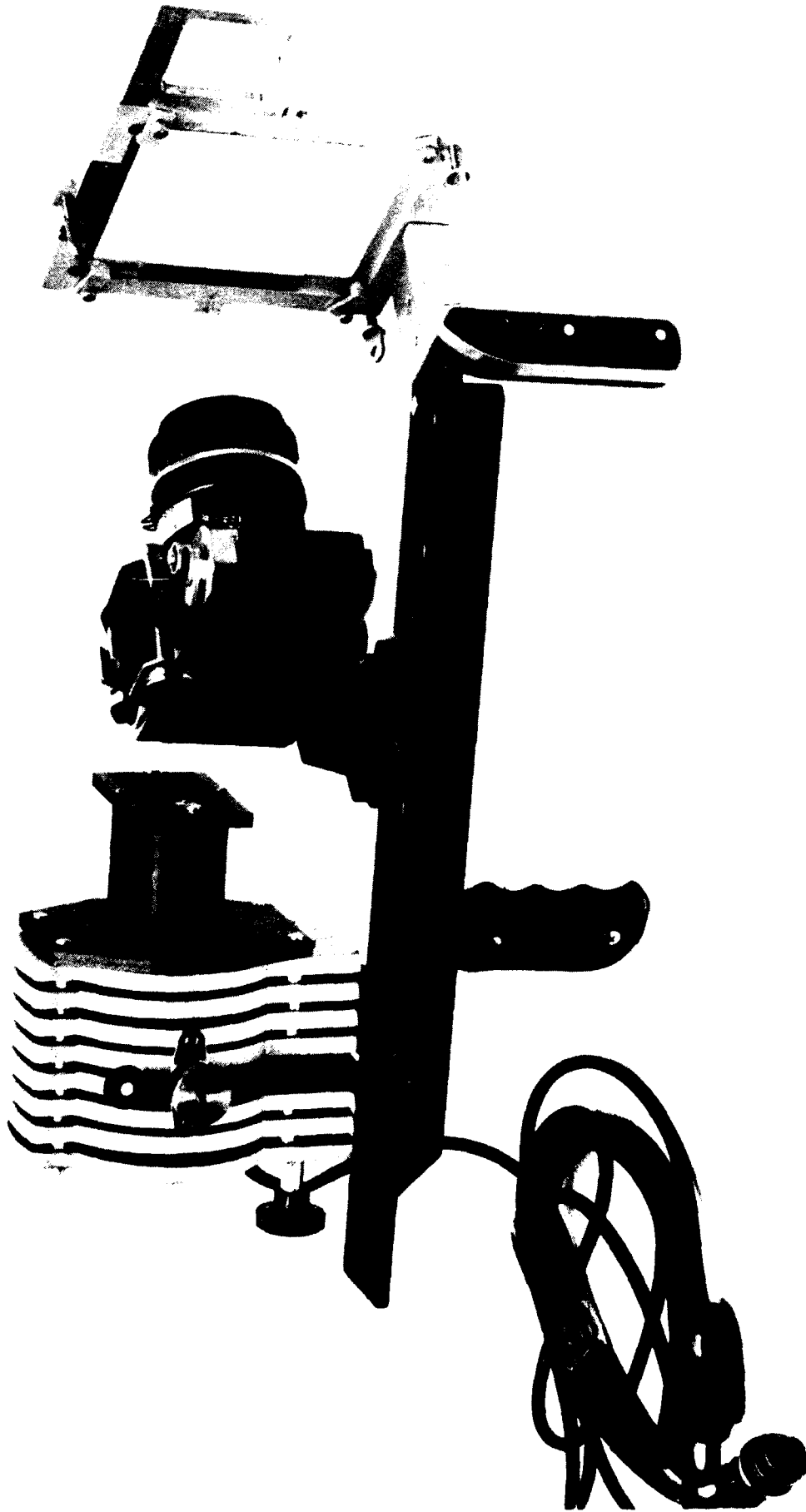


Figure 30. Photographic System for SMOPI Damage Detector

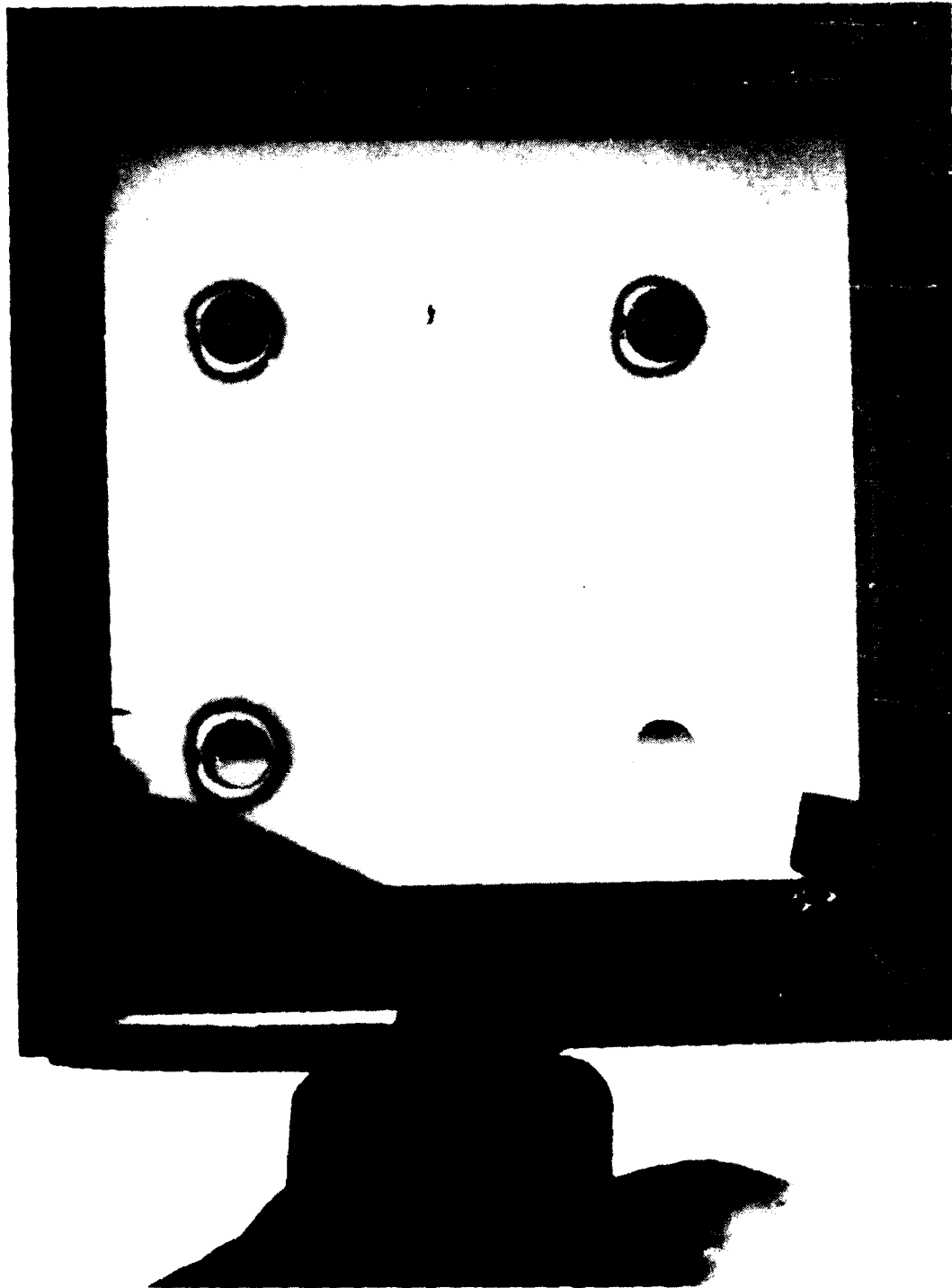


Figure 31. Cold-Worked Holes in a Metal Plate - A Fringe is Visible at Each of the Cold-Worked Holes



Figure 32. Minute Blisters in an Anti-Corrosion Paint - Visible with 150 lpi Moire Grid

NADC-90011-60
COMPOSITE REPAIR
NON-GOVERNMENT ACTIVITIES (continued)

	<u>NO. OF COPIES</u>
LTV AEROSPACE AND DEFENSE CO., Vought Missles and Advanced Programs Division, P.O. Box 6750003, Dallas, TX 75265-0003 (Attn: R. Knight, MS-TH-83).	1
LTV AEROSPACE AND DEFENSE CO., Vought Aeroproducts Division, Dallas, Texas 75265 (Attn: J. Pimm, MS 194-51).	1
LOCKHEED-CALIFORNIA CO., Burbank, CA 91510 (Attn: H. Cartmill).	1
(Attn: A. James).	1
LOCKHEED-CALIFORNIA CO., Rye Canyon Research Lab., Burbank, CA 91520 (Attn: R. C. Young).	1
LOCKHEED-GEORGIA CO., 86 South Cobb Dr., Marietta, GA 30063 (Attn: L. R. Meade, MS 399).	1
LAWRENCE LIVERMORE NATIONAL LABORATORY, P. O. Box 808, University of California/Livermore, CA 94550 (Attn: J. Brentzes).	1
MCDONNELL-DOUGLAS HELICOPTER, Culver City, CA 90230 (Attn: R. M. Verette).	1
MONOGRAM AEROSPACE FASTENERS, 3423 S. Garfield Ave., P.O. Box 6847, Los Angeles, CA 90022-0547 (Attn: F. J. Matulonis).	1
MCDONNELL-DOUGLAS ASTRONAUTICS, 5301 Bolsa Avenue, Huntington Beach, CA 92647 (Attn: C. M. Roe).	1
MCDONNELL-DOUGLAS CORP., St. Louis MO 63116 (Attn: T. Hinkle, D337/B32/L3/P370).	1
(Attn: J. Watson; G. Bilow; R. Riley).	3
(Attn: W. Shooks; C. Pingle, S. Dupay).	3
NORTHROP AIRCRAFT CORP., One Northrop Avenue, Hawthorne. CA 90250 (Attn: K. San Miguel; M. Ratwani, T. E. Steelman	3
ROCKWELL INTERNATIONAL, Columbus, OH 43216 (Attn: M. Schweiger; R. W. Gehring).	2
ROCKWELL INTERNATIONAL, P. O. Box 92098, Los Angeles, CA 90009 (Attn: G. Stewart; A. Sanders).	2
ROCKWELL INTERNATIONAL, P. O. Box 582808, Tulsa, OK 74158 (Attn: G. Sherrick; M. Whitehead).	2
ROHR INDUSTRIES, Box 878, Chula Vista, CA 92011.	1
SIKORSKY AIRCRAFT, Stratford, CT 06622 (Attn: S. Garbo; T. Cook).	2
TELEDYNE RYAN AERONAUTICAL COMPANY, 2701 Harbor Drive, P. O. Box 80311 San Diego, CA 92128 (Attn: R. Long).	1
WESTINGHOUSE ELECTRIC CORP., R&D Center, 1310 Beulah Road, Pittsburgh, PA 15235 (Attn: MS 501-3Y31, Z. Sanjana).	1

NADC-90011-60

COMPOSITE REPAIR NON-GOVERNMENT ACTIVITIES

NO. OF
COPIES

AMERICAN CYANAMID CORP., Havre de Grace, MD 21078 (Attn: R. Kreiger).	1
BEECH AIRCRAFT CORP., Claypool Bldg. Office 300, 4130 Linden Ave., Dayton, OH 45432 (Attn: M. B. Goetz).	1
BEECH AIRCRAFT CORP., Wichita, KS 67201 (Attn: M. P. Djuric).	1
BELL HELICOPTER CO., Fort Worth, TX 76101 (Attn: L. Reynolds, B. Wardlaw, M. K. Stevenson, D. M. Rhodes, and R. Rust).	5
BOEING CO., P. O. Box 3707, Seattle, WA 98124-2207 (Attn: R. Horton, 6C-11; M. Cohodas, MS 4A-16; R. June; E. T. Bannink, MS 4A-11; E. A. Westerman, MS 4R-42).	5
BOEING CO., P. O. Box 3999, Seattle, WA 98124-2207 (Attn: R. Cologne, MS 3C-23).	1
BOEING MILITARY AIRCRAFT CO., P. O. Box 7730, Wichita, KS 67277-7730 (Attn: J. Avery).	1
(Attn: J. Luding, MS K3216).	1
BOEING HELICOPTER COMPANY, P. O. Box 16858, Philadelphia, PA (Attn: P. Persaud (M/S P24-18)	1
(Attn: B. E. Lake (M/S P30-18)).	1
DOUGLAS AIRCRAFT CO., , Long Beach, CA 90846 (Attn: Dr. L. J. Hart-Smith, MS 36-90).	1
(Attn: R. Petty).	1
E. I. DUPONT DENEMOURS & CO., Centre Rd. Bldg., Wilmington, DE 19898 (Attn: Dr. P. R. Langston).	1
GENERAL DYNAMICS/CONVAIR, San Diego, CA 92138 (Attn: W. Wennhold, M. Darmody).	2
GENERAL DYNAMICS, Space Systems Division, P. O. Box 85990 San Diego, CA 92138 (Attn: Craig Rix, MZ-23-8443).	1
GENERAL DYNAMICS, P. O. Box 748, Fort Worth, TX 76101 (Attn: T. Kearns, MS 6217; M. L. Newman; B. Smith).	3
GENERAL ELECTRIC CO., P. O. Box 8555-M4018, Philadelphia, Pa 19101 (Attn: Dr. B. Rodini).	1
GENERAL ELECTRIC CO., 1 Neumann Way, Cincinnati, OH 45215 (Attn: S. Johnson/A. W. Kim).	2
GRUMMAN AEROSPACE CORP., South Oyster Bay Rd., Bethpage, L. I. NY 11714 (Attn: R. Hadcock; P. Donahue; S. Dastin).	3
HEXCEL, 11711 Dublin Blvd., P.O. Box 2312, Dublin, CA 94568-0705 (Attn: F. W. Lee).	1
HYSOL DIVISION, DEXTER CORP., P. O. Box 312, Pittsburg, CA 94565 (Attn: D. K. Klapprott).	1
KAMAN AEROSPACE, Old Windsor Road, Bloomfield, CT 06002 (Attn: A. Falcone).	1

NADC-90011-60

COMPOSITE REPAIR GOVERNMENT ACTIVITIES (continued)

	<u>NO. OF COPIES</u>
NSWC, White Oak Laboratory, Silver Spring, MD 20910	
(Attn: Dr. J. M. Augl).	1
(Attn: Dr. J. Goff, Material Evaluation Branch, Code R-34).	1
OGDEN ALC, Hill AFB, Ogden, UT 84055	
(Attn: MANEP/R. Campbell and MMETP/R. Hansen).	2
OKLAHOMA CITY ALC, Tinker AFB, Oklahoma City, OH 73145	
(Attn: MMBRE, P. Davidson and MATEE, G. Johnson).	2
ONR, 800 N. Quincy St., Arlington, VA 22217	
(Attn: A. Kushner, Code 432/A and Y. Rajapakse, Code 1132SM).	2
(Attn: R. Jones, Code 1216).	1
ONT, 800 North Quincy St., Arlington, VA 22217	
(Attn: Capt. K. Cox, ONT-21D).	1
OSD, 5203 Leesburg Pike, Falls Church VA 22041	
(Attn: P. W. Bzdak, Weapon Support Improvement Office).	1
PLASTEC, Picatinny Arsenal, Dover, NJ 07801	
(Attn: H. Peibly).	1
(Attn: Librarian, Code DRDAR-SCM-0, Bldg. 351N).	1
SACRAMENTO ALC, McClellan AFB, McClellan AFB, CA 95652	
(Attn: MANE, A. J. Hammond; MMEP, L. M. Swope and MAN, R. Orr).	3
SAN ANTONIO ALC, Kelly AFB, San Antonio, TX 78241	
(Attn: MMETM, S. Smith; MAWF, L. Kurkowski).	2
U. S. AIR FORCE ADVANCED COMPOSITES PROGRAM OFFICE, McClellan AFB, CA 95652	
(Attn: Richard B. Warnock, SM-ALC/MMEP).	1
U. S. ARMY AIR MOBILITY R&D LAB, Ft. Eustis, VA 23604	
(Attn: H. Reddick).	1
U. S. ARMY APPLIED TECHNOLOGY LAB, USARTL, (AVRADCOM), Ft. Eustis, VA 23604-5418	
(Attn: T. E. Condon).	1
ARMY MATERIALS TECHNOLOGY LABORATORY, WATERTOWN, MA 02172-0001	1
(Attn: D. Oplinger, SLCMT-MS).	1
U. S. ARMY RESEARCH OFFICE, Durham, NC 27701.	1
U. S. ARMY R&T LAB (AVRADCOM), Ames Research Center, Moffett Field, CA 94035	
(Attn: F. Immen, Code DAVDL-AS-MS 207-5).	1
U. S. ARMY R&T LAB (ARRADCOM), Bldg. 182, Dover, NJ 07801	
(Attn: K. Abelson, R. Bonk).	2
U. S. NAVAL ACADEMY, Annapolis, MD 21401	
(Attn: Mechanical Engineering Department).	1
WARNER ROBBINS ALC, ROBBINS AFB, GA 30198	
(Attn: MANE, E. A. Dykes, MMSRD, Dr. T. F. Christian and MMTRC, W. Schweinberg).	3
NAVAIRDEVCEEN, Warminster, Pa.	
(Attn: Code 6041).	20
(Attn: Code 8131).	2

NADC-90011-60

COMPOSITE REPAIR

GOVERNMENT ACTIVITIES (continued)

	NO. OF COPIES
NAVAIRENGCEN, Lakehurst, NJ 08733	
(Attn: J. Wendolowski, R. O'Donnell, Code 92A42).	2
NAVAVNDEPOT, NAS, Alameda, CA 94501	
(Attn: N. Amdur, Code 342).	1
NAVAVNDEPOT, MCAS, Cherry Point, NC 28533-5030	
(Attn: J. Meyers, Code 35110).	1
(Attn: J. Fuss, Code 35430).	1
(Attn: J. Gresham, Code 35210)).	1
NAVAVNDEPOT, NAS, Jacksonville, FL 32212-0016	
(Attn: M. Linn, Code 340).	1
NAVAVNDEPOT, NAS, Norfolk, VA 23511-5899	
(Attn: J. Deans, Code 31310; C. Garber, Code 32220).	2
(Attn: H. Sommerfleck, Code 36030).	1
NAVAVNDEPOT, NAS, North Island, San Diego, CA 92135-5112	
(Attn: D. Perl, Code 343).	1
(Attn: M. Williams, Code 31327).	1
NAVAVNDEPOT, NAS, Pensacola, FL 32508-5300	
(Attn: D. Knapp, Code 342).	1
NAVAIRSYSCOM, Washington, D.C. 20361	
(Attn: AIR-00D4).	1
(Attn: AIR-530).	1
(Attn: AIR-41113G).	1
(Attn: AIR-5302).	1
(Attn: AIR-931B).	1
(Attn: AIR-5304).	1
(Attn: AIR-5163).	1
(Attn: AIR-4103).	1
(Attn: AIR-4111).	1
(Attn: PMA 265).	1
(Attn: PMA 266).	1
(Attn: PMA 267).	1
(Attn: PMA 275).	1
NAVAL WEAPONS CENTER, China Lake, CA 93355	
(Attn: K. Bailey, J. E. Diamond).	2
NAVAVNDEPOTOPSCEN, Patuxent River, MD 20670	
(Attn: Code 313A).	1
NAVPGSCHL, Monterey, CA 93943	
(Attn: Prof. R. Ball; Prof. M. H. Bank, Prof. K. Challenger).	3
NAVSEASYSYSCOM, Washington, D. C. 20360	
(Attn: C. Zannis, SEA-05R25).	1
NSEC, Arlington, VA 20362	
(Attn: NSEC-6101E).	1
NAVSHIPRANDCEN, Bethesda, MD 20034	
(Attn: R. Rockwell, Code 1720-6).	1
NAVSHIPRANDCEN, Annapolis, MD 21401	
(Attn: H. Edelstein, Code 2870).	1
NRL, Washington, D.C. 20375	
(Attn: Code 6122 C. Poranski; Dr. I. Wolock).	2

NADC-90011-60

DISTRIBUTION LIST

COMPOSITE REPAIR GOVERNMENT ACTIVITIES

NO. OF
COPIES

AFLC, WPAFB, OH 45433	
(Attn: MAWA/T. Mallet).	1
(Attn: MAQI/L. Hary).	1
AFALC, WPAFB, OH 45433-5001	
(Attn: PTE/J. Yanker).	1
AFWAL, WPAFB, OH 45433-6553	
(Attn: FIBEC, Dr. G. Sendeckyj).	1
(Attn: FIBC/L. Kelly).	1
(Attn: FIBCA/C. Ramsey).	1
(Attn: FIBG/H. F. Wolfe).	1
(Attn: FIBA/W. Goesch).	1
AFWAL, WPAFB, OH 45433-6533	
(Attn: MLBM/Dr. J. Whitney, M. Knight).	2
(Attn: MLB/F. Cherry).	1
(Attn: MBC/J. Reinhart).	1
(Attn: MLJ/W. Scardino).	1
(Attn: MLSE/M. Forte).	1
(Attn: MLTN/R. C. Tomashot).	1
COMLATWINGPAC, NAS, Lemoore, CA 93245	
(Attn: Lt. R. B. Crisler, Code 77).	1
COMNAVAIRLANT, NAS, Norfolk, VA 23511	
(Attn: Code 5281/G. T. Browne).	1
COMNAVAIRPAC, NAS, North Island, San Diego, CA 92135	
(Attn: Code 7412/B. Fusco).	1
CORPUS CHRISTI ARMY DEPOT, Corpus Christi, TX 78419	
(Attn: Doug Patterson/Don Wells, SDSCC/MPI).	2
DEPARTMENT OF THE AIR FORCE, Bldg. 410, Bolling Air Force Base Washington, D.C. 20332	
(Attn: Dr. M. Salkind, Dr. Amos).	2
DEFENSE TECHNICAL INFORMATION CENTER (DTIC), Bldg. #5, Cameron Station, Alexandria, VA 22314	
(Attn: Administrator).	2
FAA, Washington, D. C. 20591	
(Attn: J. R. Soderquist).	1
FAA, Technical Center, Atlantic City, NJ 08405	
(Attn: L. Neri, Code ACT-330; C. Caiafa, Code ACT-330).	2
NASA, Langley Research Center, Hampton, VA 23365-5225	
(Attn: Mr. C. E. Harris, MS 188E; Dr. J. Starnes, MS 190; Dr. M. Mikulus, Mr. H. Bohan, MS 189M; J. W. Deaton, MS 188A; Dr. R. Price, Dr. G. L. Roderick).	7
NASA Headquarters, Washington, D. C. 20546	
(Attn: Airframes Branch, FS 120).	1
(Attn: OAST/RM, Dr. Daniel Mulville).	1
NASA, Lewis Research Center, Cleveland, OH 44153	
(Attn: Technical Library).	1
NASA, George C. Marshall Space Flight Center, Huntsville, AL 35812	
(Attn: Technical Library).	1